

Loss of p53 triggers WNT-dependent systemic inflammation to drive breast cancer metastasis

Max D. Wellenstein^{1,10}, Seth B. Coffelt^{1,8,9,10}, Danique E. M. Duits¹, Martine H. van Miltenburg², Maarten Slagter^{3,4}, Iris de Rink⁵, Linda Henneman⁶, Sjors M. Kas², Stefan Prekovic⁷, Cheei-Sing Hau¹, Kim Vrijland¹, Anne Paulien Drenth², Renske de Korte-Grimmerink⁶, Eva Schut², Ingrid van der Heijden², Wilbert Zwart⁷, Lodewyk F. A. Wessels⁴, Ton N. Schumacher³, Jos Jonkers^{2*} & Karin E. de Visser^{1*}

Cancer-associated systemic inflammation is strongly linked to poor disease outcome in patients with cancer^{1,2}. For most human epithelial tumour types, high systemic neutrophil-to-lymphocyte ratios are associated with poor overall survival³, and experimental studies have demonstrated a causal relationship between neutrophils and metastasis^{4,5}. However, the cancer-cell-intrinsic mechanisms that dictate the substantial heterogeneity in systemic neutrophilic inflammation between tumour-bearing hosts are largely unresolved. Here, using a panel of 16 distinct genetically engineered mouse models for breast cancer, we uncover a role for cancer-cell-intrinsic p53 as a key regulator of pro-metastatic neutrophils. Mechanistically, loss of p53 in cancer cells induced the secretion of WNT ligands that stimulate tumour-associated macrophages to produce IL-1β, thus driving systemic inflammation. Pharmacological and genetic blockade of WNT secretion in p53-null cancer cells reverses macrophage production of IL-1β and subsequent neutrophilic inflammation, resulting in reduced metastasis formation. Collectively, we demonstrate a mechanistic link between the loss of p53 in cancer cells, secretion of WNT ligands and systemic neutrophilia that potentiates metastatic progression. These insights illustrate the importance of the genetic makeup of breast tumours in dictating pro-metastatic systemic inflammation, and set the stage for personalized immune intervention strategies for patients with cancer.

To determine how pro-metastatic systemic inflammation is influenced by genetic aberrations in tumours, we studied 16 genetically engineered mouse models (GEMMs) for breast cancer carrying different tissue-specific mutations. These GEMMs represent most subtypes of human breast cancer, including ductal and lobular carcinoma, oestrogen receptor-positive (luminal A), HER2⁺, triple-negative and basal-like breast cancer. Because we and others have demonstrated that neutrophils expand systemically and promote metastasis^{5–10}, we evaluated circulating levels of neutrophils as a marker for systemic inflammation in mammary tumour-bearing mice with end-stage disease. As expected, most tumour-bearing mice displayed an increase in circulating neutrophils compared with non-tumour-bearing wild-type animals (Fig. 1a). Like the inter-patient heterogeneity in systemic inflammation in human breast cancer¹¹, we observed a striking variability in the extent of neutrophilia between the different tumour-bearing GEMMs (Fig. 1a, Extended Data Fig. 1a). We found that the models exhibiting high neutrophil expansion displayed a subset of neutrophils expressing the stem-cell marker cKIT (Fig. 1b), indicative of an immature neutrophil phenotype⁵. We subsequently searched for commonalities and differences among the 16 GEMMs with regards to high versus low levels of systemic neutrophils. Notably, mice bearing tumours with

a p53 deletion exhibited the most pronounced levels of circulating neutrophils (Fig. 1a). The difference in the magnitude of systemic inflammation between p53-proficient and p53-null tumours was even more apparent when focusing on cKIT⁺ neutrophils (Fig. 1b).

In mouse models for colorectal, pancreatic, prostate and endometrial cancer, p53 mutation or loss leads to recruitment and activation of immune cells in the primary tumour microenvironment^{12–16}. To study the association between p53 status of the tumour and systemic inflammation, we separated the 16 GEMMs based on the presence or absence of homozygously floxed *Trp53* alleles and compared the levels of circulating neutrophils and the proportion of cKIT-expressing neutrophils. This analysis confirmed a statistically significant difference between mice bearing p53-proficient and p53-null tumours (Fig. 1c, d).

We previously demonstrated that expansion of neutrophils in mammary tumour-bearing *Krt14*(*K14*)-*cre*; *Cdh1*^{F/F}; *Trp53*^{F/F} (KEP) mice is driven by an inflammatory pathway that involves CCL2, IL-1β, IL-17A and granulocyte colony-stimulating factor (G-CSF)^{5,17}. We found that serum levels of CCL2, IL-1β and G-CSF correlated with p53 loss in primary tumours in the 16 GEMMs (Fig. 1e–h). Principal component analysis of these systemic immune parameters further demonstrated that systemic inflammation correlated with the p53 status of the tumour (Fig. 1i).

To provide evidence for a causal relationship between p53 loss in mammary tumours and neutrophilia, we derived cancer cell lines from two independent p53-proficient tumour models—*Wap*-*cre*; *Cdh1*^{F/F}; *Akt1*^{E17K} (WEA)¹⁸ and *Wap*-*cre*; *Cdh1*^{F/F}; *Pik3ca*^{E545K} (WEP). Using CRISPR-Cas9-mediated gene disruption, we targeted *Trp53*, which resulted in an inability to increase p21 levels after irradiation (Extended Data Fig. 2a, b, e). We orthotopically transplanted WEA; *Trp53*^{+/-} and WEP; *Trp53*^{+/-} cells, and matched WEA; *Trp53*^{-/-} and WEP; *Trp53*^{-/-} cells into syngeneic wild-type mice (Fig. 2a). Although the loss of p53 conferred a proliferation advantage in vitro, growth kinetics in vivo were similar between p53-proficient and p53-deficient tumours for both cell lines (Extended Data Fig. 2c–g). Consistent with our findings in the GEMM panel, we observed increased expansion of neutrophils, including cKIT⁺ neutrophils, in the circulation and lungs of mice bearing WEA; *Trp53*^{-/-} and WEP; *Trp53*^{-/-} tumours, when compared with mice bearing size-matched p53-proficient tumours (Fig. 2b–d, Extended Data Fig. 2h, i). In addition, mice with WEA; *Trp53*^{-/-}, but not WEP; *Trp53*^{-/-}, tumours presented with splenomegaly when compared with *Trp53*^{+/-} controls (Extended Data Fig. 2j)—a phenomenon often observed in inflammation and cancer¹⁹. These data reveal that the loss of p53 in breast cancer cells is a central driving event of cancer-induced systemic neutrophilic inflammation.

¹Division of Tumour Biology & Immunology, Oncode Institute, Netherlands Cancer Institute, Amsterdam, The Netherlands. ²Division of Molecular Pathology, Oncode Institute, Netherlands Cancer Institute, Amsterdam, The Netherlands. ³Division of Molecular Oncology & Immunology, Oncode Institute, Netherlands Cancer Institute, Amsterdam, The Netherlands. ⁴Division of Molecular Carcinogenesis, Oncode Institute, Netherlands Cancer Institute, Amsterdam, The Netherlands. ⁵Genomics Core Facility, Netherlands Cancer Institute, Amsterdam, The Netherlands. ⁶Mouse Clinic for Cancer and Aging, Netherlands Cancer Institute, Amsterdam, The Netherlands. ⁷Division of Oncogenomics, Oncode Institute, Netherlands Cancer Institute, Amsterdam, The Netherlands. ⁸Present address: Institute of Cancer Sciences, University of Glasgow, Glasgow, UK. ⁹Present address: Cancer Research UK Beatson Institute, Glasgow, UK. ¹⁰These authors contributed equally: Max D. Wellenstein, Seth B. Coffelt. *e-mail: j.jonkers@nki.nl; k.d.visser@nki.nl

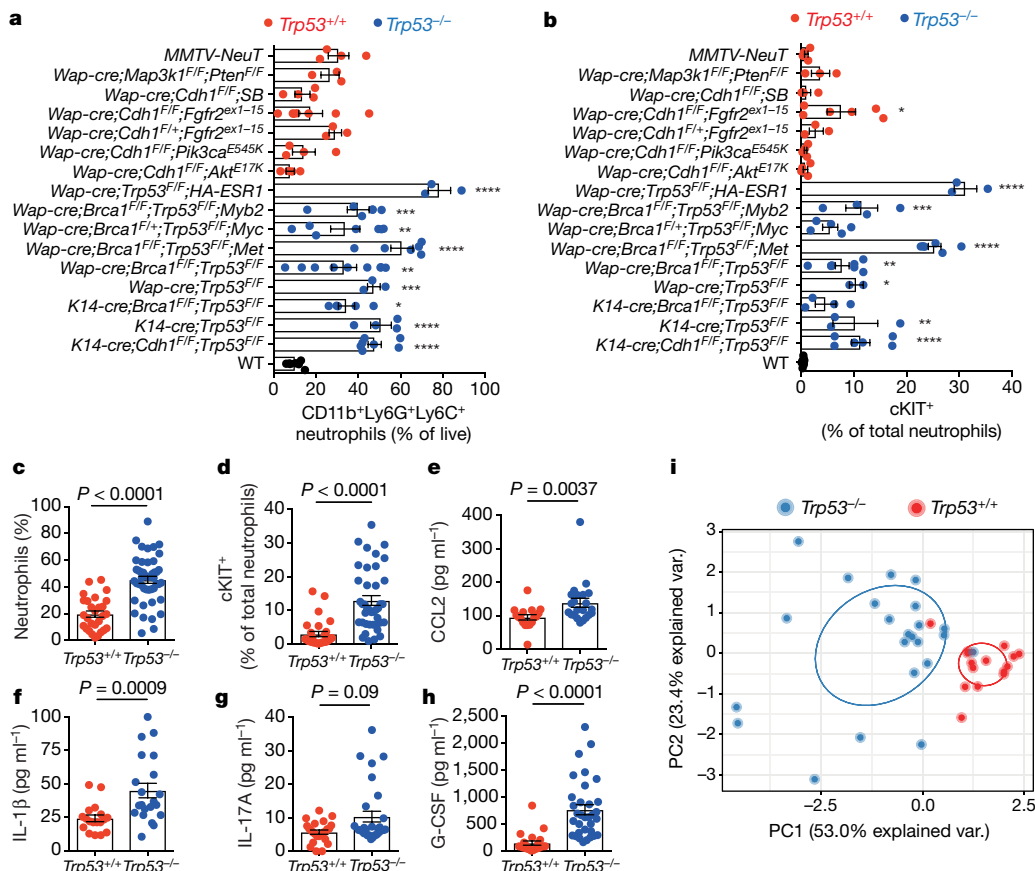


Fig. 1 | Loss of p53 in mammary cancer cells correlates with systemic neutrophilic inflammation. **a, b**, Flow cytometry analysis of frequency of CD11b⁺Ly6G⁺Ly6C⁺ neutrophils (**a**) and proportion of cKIT⁺ neutrophils (**b**) as determined by flow cytometry analysis on blood of breast cancer GEMMs at end stage (cumulative tumour volume 1,500 mm³) and non-tumour-bearing (wild-type; WT) controls ($n = 4$, 3, 4, 7, 3, 4, 4, 3, 6, 7, 6, 9, 3, 5, 4, 7 and 7 mice, top to bottom). * $P < 0.05$, ** $P < 0.01$, *** $P < 0.001$, **** $P < 0.0001$, compared to wild-type control by two-tailed one-way analysis of variance (ANOVA) with Tukey's multiple-testing correction. **c, d**, Total neutrophil frequencies (**c**) and

cKIT⁺ neutrophil frequencies (**d**) in circulation of all *Trp53^{+/+}* ($n = 28$) and *Trp53^{-/-}* ($n = 46$) tumour-bearing mice, combined from **a** and **b**. **e–h**, CCL2 levels ($n = 17$ *Trp53^{+/+}*, $n = 22$ *Trp53^{-/-}*) (**e**), IL-1 β levels ($n = 18$ *Trp53^{+/+}*, $n = 21$ *Trp53^{-/-}*) (**f**), IL-17A levels ($n = 24$ *Trp53^{+/+}*, $n = 30$ *Trp53^{-/-}*) (**g**) and G-CSF levels ($n = 22$ *Trp53^{+/+}*, $n = 33$ *Trp53^{-/-}*) (**h**) in serum of GEMMs at end stage based on p53 status. P values in **c–h** determined by two-tailed Mann–Whitney *U*-test. **i**, Principal component analysis of data depicted in **a–h** (13 out of 16 GEMMs). Each symbol represents one mouse. Circles contour 40% of group-specific Gaussian probability distributions of sample scores. All data are mean \pm s.e.m.

Because we observed cKIT⁺ immature neutrophils in p53-null tumour-bearing mice (Figs 1d, 2d), we next investigated whether haematopoiesis was altered. In mice bearing *WEA;Trp53^{-/-}* tumours, the frequencies of Lin⁻Sca1⁺cKIT⁺ cells, common myeloid progenitors, CD11b⁺Ly6G^{low} pro-myelocytes and mature neutrophils were increased in the bone marrow at the expense of megakaryocyte and erythrocyte progenitors, when compared to *WEA;Trp53^{+/+}* tumour-bearing mice (Extended Data Fig. 3a–c). This effect on cell proportions was not reflected in the total cell counts, possibly owing to a slight depletion of total bone marrow cell numbers in *WEA;Trp53^{-/-}* tumour-bearing mice (Extended Data Fig. 3d).

Previously, we reported that macrophage-derived IL-1 β in the tumour microenvironment triggers systemic neutrophil expansion in KEP mice⁵. Because serum levels of IL-1 β correlated with p53 status (Fig. 1f), we proposed that loss of p53 changes the secretome of cancer cells, stimulating IL-1 β production from tumour-associated macrophages (TAMs) and setting off a systemic inflammatory cascade. Indeed, in vitro exposure of bone marrow-derived macrophages (BMDMs) to conditioned medium from *WEA;Trp53^{-/-}* or *WEA;Trp53^{+/+}* cancer cells differentially affected their phenotype (Extended Data Fig. 4a). Notably, conditioned medium from *WEA;Trp53^{-/-}* and *WEP;Trp53^{-/-}* cells strongly induced *Il1b* mRNA expression in cultured BMDMs compared with conditioned medium from matched *Trp53^{+/+}* controls (Fig. 2e). In agreement with our mouse data, human monocyte-derived macrophages (MDMs) cultured

with tumour conditioned medium of *TP53^{-/-}* MCF-7 human breast cancer cells displayed increased CD206 and CD163 expression compared with human MDMs cultured with conditioned medium of p53-proficient MCF-7 cells (Extended Data Fig. 4c). We also observed increased *IL1B* expression in human MDMs after exposure to *TP53^{-/-}* MCF-7 cells compared with *TP53^{+/+}* controls (Extended Data Fig. 4d). These data indicate that cancer-cell-intrinsic p53 status dictates the crosstalk between cancer cells and macrophages in a paracrine fashion, resulting in an altered macrophage phenotype and IL-1 β production. We also observed increased levels of *IL1B* mRNA expression in breast tumours of The Cancer Genome Atlas (TCGA) with mutations in *TP53* compared with wild-type *TP53* tumours (Fig. 2f), suggesting similar p53-dependent activation of IL-1 β signalling in human breast cancer.

To identify which factor(s) in p53-null tumours mediate TAM activation and subsequent systemic inflammation, we performed RNA sequencing on mammary tumours of 12 different GEMMs (7 p53-deficient tumours, 5 p53-proficient tumours; 145 tumours in total). The p53-deficient tumours differed substantially from p53-proficient tumours in terms of gene expression, regardless of any additional genetic aberrations, demonstrating a dominant effect of p53 loss on the global transcriptome (Extended Data Fig. 5a). Interestingly, the most significantly changed pathways in p53-deficient tumours pertained to adaptive immune phenotypes (Fig. 3a). Although neutrophil and TAM numbers were altered intratumourally, the composition of CD8⁺, CD4⁺ or FOXP3⁺ T cells did not correlate with p53 status (Extended Data

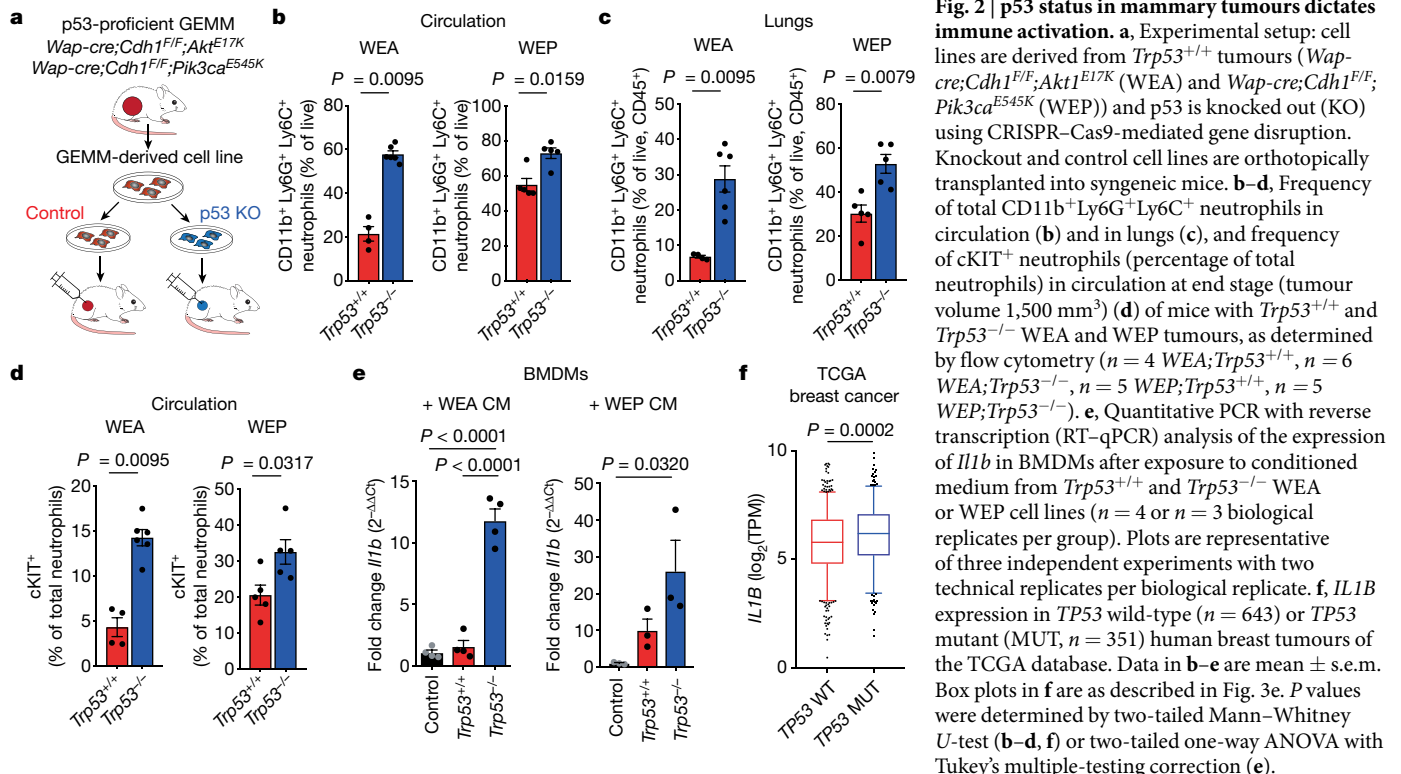


Fig. 5b–g), suggesting that the distinct transcriptome profiles are not due to a p53-dependent effect on the composition of the adaptive immune landscape.

From the Gene Ontology analysis, we selected genes that encode secreted factors that could potentially influence TAMs. One of the

upregulated pathways in p53-null tumours included WNT and β -catenin signalling (Fig. 3a). WNT signalling is linked to the production of IL-1 β in acute arthritis, as well as immune and stromal signalling in cancer^{20–23}. Using a WNT and β -catenin signalling gene signature, we found that p53-null GEMM tumours clustered separately from

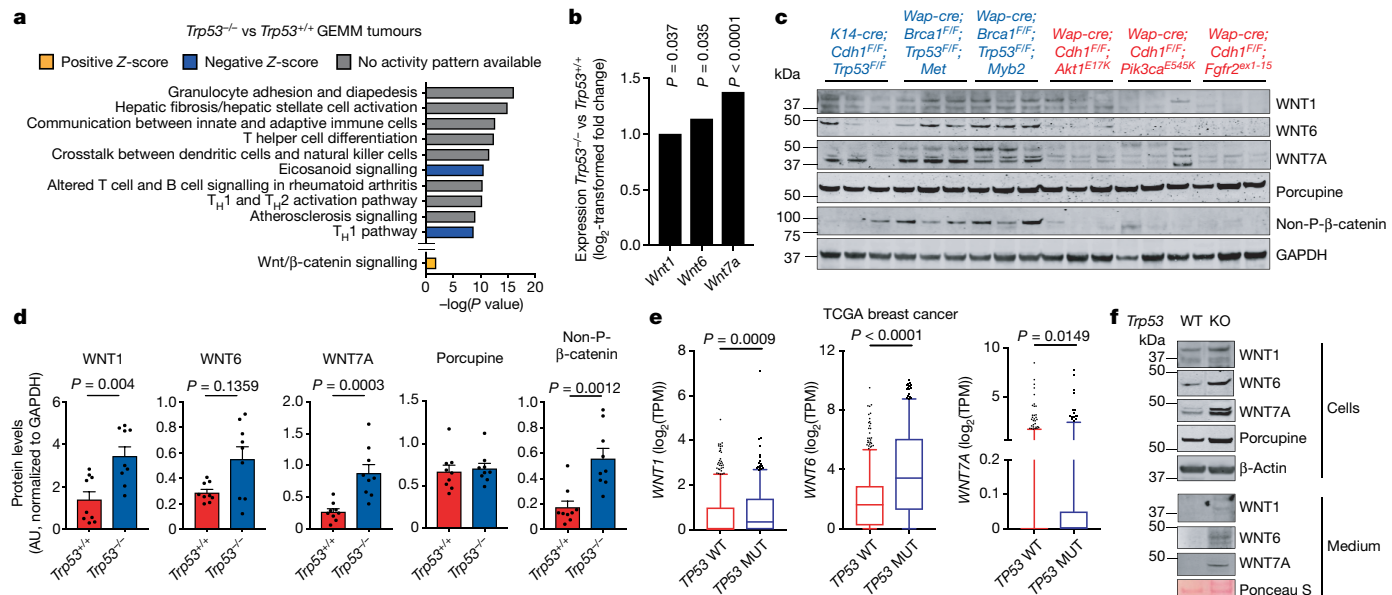


Fig. 1. **d**, Quantification of results in **c** ($n = 3$ per group). Data are mean \pm s.e.m. **e**, Expression of *WNT1*, *WNT6* and *WNT7A* in *TP53* wild-type ($n = 643$) and mutant ($n = 351$) human breast tumours of the TCGA breast cancer database. Box plots show the 5th to 95th percentiles, with median and quartiles indicated. **f**, Western blot analysis on cell lysate and conditioned medium of *Wap-cre; Cd11^{F/F}; Akt1^{E17K}; Trp53^{+/+}* (WT) and *Wap-cre; Cd11^{F/F}; Akt1^{E17K}; Trp53^{-/-}* (KO) cell lines for WNT ligands. Representative of two independent experiments. *P* values were determined by two-tailed one-way ANOVA, with false discovery rate (FDR) multiple-testing correction (**b**) or two-tailed Mann–Whitney *U*-test (**d**, **e**).

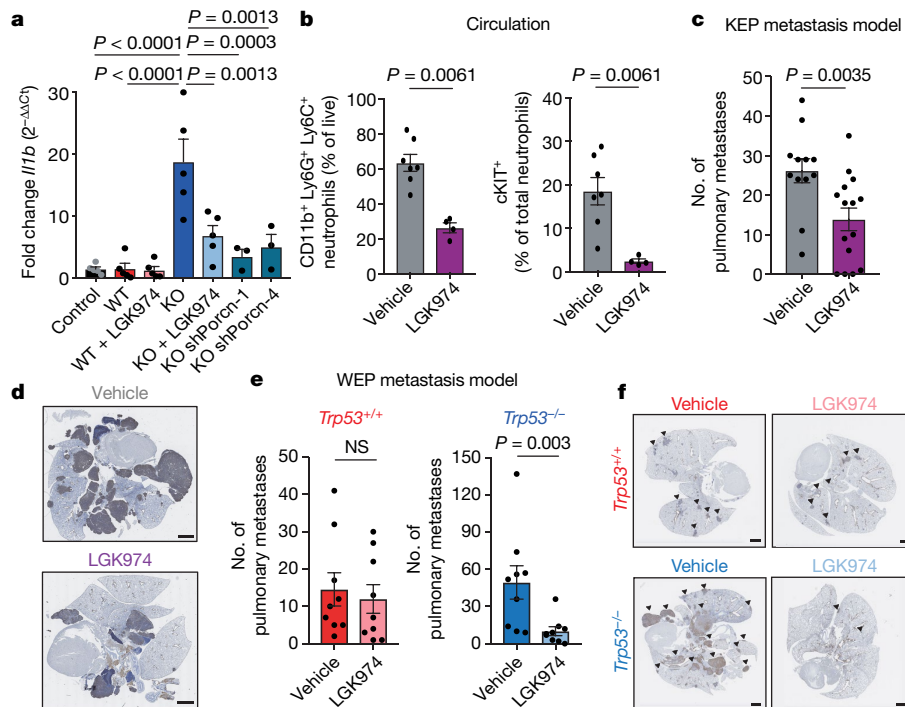


Fig. 4 | WNT-induced systemic inflammation promotes metastasis of p53-null tumours. **a**, RT-qPCR analysis of BMDMs after exposure to control medium or conditioned medium from *Wap-cre; Cdh1^{FF}; Akt1^{E17K}; Trp53^{+/+}* (WT), *Wap-cre; Cdh1^{FF}; Akt1^{E17K}; Trp53^{-/-}* (KO) or *Wap-cre; Cdh1^{FF}; Akt1^{E17K}; Trp53^{-/-}* cells transduced with two independent shRNAs against *Porcn* (KO shPorcn-1 and shPorcn-4). Where indicated, cell lines were pre-treated with 1 μM LGK974 ($n = 5$ biological replicates per group for WT, WT + LGK974, KO and KO + LGK974, $n = 3$ biological replicates for KO shPorcn-1 and KO shPorcn-4). Plots are representative of three separate experiments, with two technical replicates per biological replicate. **b**, Frequency of total CD11b⁺Ly6G⁺Ly6C⁺ neutrophils and cKIT⁺ neutrophils in the circulation of *K14-cre; Cdh1^{FF}; Trp53^{FF}* (KEP) mice after 5 days of LGK974 ($n = 4$) or vehicle ($n = 7$) treatment starting at a tumour volume of 500 mm^3 . **c**, Number of

pulmonary metastases after KEP tumour-bearing mice were treated with LGK974 ($n = 15$) or vehicle ($n = 12$). KEP tumour fragments were orthotopically transplanted in FVB/N mice and treatment was initiated when tumours were 30–40 mm^3 and continued until primary tumour removal. **d**, Representative images of cytokeratin-8 staining of lungs of KEP tumour-bearing mice. Scale bars, 1.9 mm. **e**, Number of pulmonary metastases after orthotopic injection of *Trp53^{+/+}* and *Trp53^{-/-}* WEP cells and treatment with LGK974 or vehicle ($n = 9$ per group). Treatment was initiated when tumours were 30–40 mm^3 and continued until 1,500 mm^3 . **f**, Representative images of cytokeratin-8 staining of lungs of WEP tumour-bearing mice, arrows indicate examples of metastatic nodules. Scale bars, 1.4 mm. All data are mean \pm s.e.m. P values were determined by two-tailed one-way ANOVA with Tukey's multiple-testing correction (a) or two-tailed Mann-Whitney U-test (b, c, e). NS, not significant.

p53-proficient tumours, indicating an association between loss of p53 and WNT-related gene expression (Extended Data Fig. 6a, b). Many WNT-related genes were upregulated in p53-deficient tumours, including three WNT ligands, *Wnt1*, *Wnt6* and *Wnt7a*, whereas the expression of negative regulators of WNT signalling was decreased (Fig. 3b, Extended Data Fig. 6c). Increased protein levels of WNT1 and WNT7A were confirmed in a set of independent p53-deficient tumours (Fig. 3c, d). We also found increased expression of non-phosphorylated β -catenin, indicative of activated WNT signalling (Fig. 3c, d). In human breast tumours, expression of WNT1, WNT6 and WNT7A was increased after aberrant expression of *TP53*, compared with wild-type *TP53* tumours (Fig. 3e). We then broadened our analysis of TCGA data to other WNT-related genes and discovered a trend towards enrichment of these genes in *TP53*-mutated tumours (Extended Data Fig. 6d). In addition, individual WNT-stimulating genes were upregulated, whereas WNT-inhibiting genes were downregulated in mutant versus wild-type *TP53* human tumours (Extended Data Fig. 6e), indicating that WNT signalling is activated after aberrant expression of *TP53*. Using WEA cell lines, we confirmed that the WNT1, WNT6 and WNT7A proteins are increased intracellularly in *WEA; Trp53^{-/-}* cells and secreted, when compared with *WEA; Trp53^{+/+}* cells (Fig. 3f). Collectively, these data indicate cancer-cell-autonomous secretion of WNT ligands after loss of p53.

Because deletion of p53 increases WNT ligand expression, we proposed that wild-type p53 negatively regulates these genes, either directly or indirectly. To determine whether p53 binds the regulatory regions of *Wnt1*, *Wnt6* and/or *Wnt7a*, we performed chromatin

immunoprecipitation followed by high-throughput sequencing (ChIP-seq) in three independent WEA and WEP cell lines. p53 binding was observed at the *Cdkn1a* (p21) locus (Extended Data Fig. 7a), whereas we did not find p53 binding at the *Wnt1*, *Wnt6* or *Wnt7a* loci (Extended Data Fig. 7b), suggesting that p53 regulates their expression indirectly. Because p53 has been described to control *Wnt1* expression by activating microRNA-34a (miR-34a)²⁴, we wondered whether this microRNA may be involved in the regulation of *Wnt1*, *Wnt6* and *Wnt7a*. Indeed, we observed p53 chromatin binding at the miR-34a locus in all cell lines (Extended Data Fig. 7c). Overexpression of miR-34a in *WEA; Trp53^{-/-}* cells resulted in a significant reduction of WNT ligand expression (Extended Data Fig. 7d). These data suggest that wild-type p53 negatively regulates the expression of *Wnt1*, *Wnt6* and *Wnt7a* via miR-34a.

We then assessed the role of cancer-cell-derived WNT ligands on IL-1 β production by macrophages. We treated WEA cells with LGK974—which inhibits porcupine (encoded by *Porcn*), a WNT-specific acyltransferase that regulates WNT ligand secretion²⁵—and added conditioned medium to macrophages. LGK974 reduced the *WEA; Trp53^{-/-}* cell-induced *Il1b* expression by macrophages (Fig. 4a). We also depleted *Porcn* in *WEA; Trp53^{-/-}* cells using short hairpin RNAs (shRNAs), which resulted in reduced macrophage expression of *Il1b*, consistent with pharmacological inhibition of porcupine (Fig. 4a). These data confirm a causal relationship between WNT ligand secretion by p53-deficient cancer cells and IL-1 β expression in macrophages.

To identify the receptors involved in the crosstalk between p53-null cancer cells and macrophages, we looked for genes that encode WNT receptors in the GEMM gene expression data. We found that

Frizzled receptors, *Fzd7* and *Fzd9*, were upregulated in the p53-null tumours compared with p53-proficient tumours (Extended Data Fig. 8a). Similarly, expression of *FZD7* and *FZD9* was increased in mutant *TP53* human breast tumours compared with wild-type *TP53* tumours (Extended Data Fig. 8b). We then used small interfering RNAs (siRNAs) to knockdown both *Fzd7* and *Fzd9* in BMDMs (Extended Data Fig. 8c), which prevented induction of *Il1b* by *WEA;Trp53^{-/-}* cells (Extended Data Fig. 8d), demonstrating that FZD7 and FZD9 are involved in WNT-induced activation of macrophages in vitro.

We next assessed whether the production of WNT ligands by p53-deficient cancer cells drives systemic inflammation. We treated tumour-bearing KEP mice with LGK974 for five consecutive days, and this led to a reduction in the levels of total neutrophils and cKIT⁺ neutrophils in blood and lungs when compared with vehicle-treated KEP mice (Fig. 4b, Extended Data Fig. 9a). In addition, IL-17A-producing γδ T cells—the key cell type responding to IL-1β that drives neutrophil accumulation and consequently metastasis⁵—were reduced in the lungs of LGK974-treated KEP mice (Extended Data Fig. 9b), indicating that γδ T cell activation upstream of pro-metastatic neutrophil accumulation depends on WNT signalling. Similarly, long-term treatment of KEP mice with LGK974 blocked neutrophil expansion over time (Extended Data Fig. 9c). To exclude the possibility that the observed reduction in inflammation is a result of targeting non-tumour cells by LGK974, we orthotopically transplanted *WEA;Trp53^{-/-};shPorcn* cell lines and matched *WEA;Trp53^{-/-};shControl* cells into wild-type mice. Analysis of size-matched end-stage tumours revealed an incomplete reduction of *Porcn* expression (Extended Data Fig. 9d). Although we cannot formally exclude the possibility that non-cancer cells contribute to the residual *Porcn* expression, expression levels of *Porcn* in the tumours correlated with levels of circulating neutrophils, cKIT⁺ neutrophils and *Il1b* expression (Extended Data Fig. 9e–g). Moreover, knockdown of *Porcn* prevented splenomegaly (Extended Data Fig. 9h). Collectively, these data confirm the causal link between WNT secretion triggered by p53-deficient mammary tumours and systemic inflammation.

Because the γδ T cell–neutrophil axis promotes metastasis^{4,5} and these cells are regulated by WNT ligands, we proposed that LGK974 treatment may present a viable therapeutic strategy to inhibit metastasis of p53-null mammary tumours. To test this, we treated KEP tumour-bearing mice with LGK974 or vehicle, after which we surgically removed the primary tumour and assessed metastatic progression. Notably, although blockade of porcupine did not affect the growth of primary tumours (Extended Data Fig. 9i), pulmonary metastases were reduced (Fig. 4c, d). In an independent metastasis model in which we orthotopically transplanted matched *Trp53^{+/+}* and *Trp53^{-/-}* WEP cell lines, we observed that the absence of p53 increases lung metastasis formation (Fig. 4e, left and right graphs; $P = 0.0153$). We then treated both *WEP;Trp53^{+/+}* and *WEP;Trp53^{-/-}* tumour-bearing mice with LGK974, which failed to influence primary tumour growth (Extended Data Fig. 9j). However, LGK974 treatment reduced metastasis of *WEP;Trp53^{-/-}* tumours, without affecting metastasis of *WEP;Trp53^{+/+}* tumours (Fig. 4e, f). These data show that blocking WNT-induced systemic inflammation impedes metastasis formation of p53-null mammary tumours.

In summary, we show that the status of p53 is an important driver of systemic pro-metastatic inflammation in breast cancer (Extended Data Fig. 9k) and that targeting WNT signalling may represent a promising therapeutic modality for patients with p53-deficient breast tumours. Together with recent literature on the importance of canonical driver mutations in shaping the local immune composition of primary tumours²⁶, our findings shed light on the poorly understood inter-patient heterogeneity in the systemic composition and function of immune cells. Mechanistic understanding of the intricate interactions between cancer-cell-intrinsic genetic events and the immune landscape provides a basis for the design of personalized immune intervention strategies for patients with cancer.

Online content

Any methods, additional references, Nature Research reporting summaries, source data, extended data, supplementary information, acknowledgements, peer review information; details of author contributions and competing interests; and statements of data and code availability are available at <https://doi.org/10.1038/s41586-019-1450-6>.

Received: 15 February 2018; Accepted: 26 June 2019;

Published online 31 July 2019.

- Diakos, C. I., Charles, K. A., McMillan, D. C. & Clarke, S. J. Cancer-related inflammation and treatment effectiveness. *Lancet Oncol.* **15**, e493–e503 (2014).
- McAllister, S. S. & Weinberg, R. A. The tumour-induced systemic environment as a critical regulator of cancer progression and metastasis. *Nat. Cell Biol.* **16**, 717–727 (2014).
- Templeton, A. J. et al. Prognostic role of neutrophil-to-lymphocyte ratio in solid tumors: a systematic review and meta-analysis. *J. Natl. Cancer Inst.* **106**, dju124 (2014).
- Coffelt, S. B., Wellenstein, M. D. & de Visser, K. E. Neutrophils in cancer: neutral no more. *Nat. Rev. Cancer* **16**, 431–446 (2016).
- Coffelt, S. B. et al. IL-17-producing γδ T cells and neutrophils conspire to promote breast cancer metastasis. *Nature* **522**, 345–348 (2015).
- Kowanetz, M. et al. Granulocyte-colony stimulating factor promotes lung metastasis through mobilization of Ly6G⁺/Ly6C⁺ granulocytes. *Proc. Natl Acad. Sci. USA* **107**, 21248–21255 (2010).
- Bald, T. et al. Ultraviolet-radiation-induced inflammation promotes angiogenesis and metastasis in melanoma. *Nature* **507**, 109–113 (2014).
- Wculek, S. K. & Malanchi, I. Neutrophils support lung colonization of metastasis-initiating breast cancer cells. *Nature* **528**, 413–417 (2015).
- Park, J. et al. Cancer cells induce metastasis-supporting neutrophil extracellular DNA traps. *Sci. Transl. Med.* **8**, 361ra138 (2016).
- Steele, C. W. et al. CXCR2 inhibition profoundly suppresses metastases and augments immunotherapy in pancreatic ductal adenocarcinoma. *Cancer Cell* **29**, 832–845 (2016).
- Ethier, J. L., Desautels, D., Templeton, A., Shah, P. S. & Amir, E. Prognostic role of neutrophil-to-lymphocyte ratio in breast cancer: a systematic review and meta-analysis. *Breast Cancer Res.* **19**, 2 (2017).
- Cooks, T. et al. Mutant p53 prolongs NF-κB activation and promotes chronic inflammation and inflammation-associated colorectal cancer. *Cancer Cell* **23**, 634–646 (2013).
- Schwitalia, S. et al. Loss of p53 in enterocytes generates an inflammatory microenvironment enabling invasion and lymph node metastasis of carcinogen-induced colorectal tumors. *Cancer Cell* **23**, 93–106 (2013).
- Stodden, G. R. et al. Loss of *Cdh1* and *Trp53* in the uterus induces chronic inflammation with modification of tumor microenvironment. *Oncogene* **34**, 2471–2482 (2015).
- Wörmann, S. M. et al. Loss of p53 function activates JAK2-STAT3 signaling to promote pancreatic tumor growth, stroma modification, and gemcitabine resistance in mice and is associated with patient survival. *Gastroenterology* **151**, 180–193 (2016).
- Bezzi, M. et al. Diverse genetic-driven immune landscapes dictate tumor progression through distinct mechanisms. *Nat. Med.* **24**, 165–175 (2018).
- Kersten, K. et al. Mammary tumor-derived CCL2 enhances pro-metastatic systemic inflammation through upregulation of IL1β in tumor-associated macrophages. *OncolImmunology* **6**, e1334744 (2017).
- Annunziato, S. et al. Modeling invasive lobular breast carcinoma by CRISPR/Cas9-mediated somatic genome editing of the mammary gland. *Genes Dev.* **30**, 1470–1480 (2016).
- Song, X. et al. CD11b⁺/Gr-1⁺ immature myeloid cells mediate suppression of T cells in mice bearing tumors of IL-1β-secreting cells. *J. Immunol.* **175**, 8200–8208 (2005).
- Singh, V., Holla, S., Ramachandra, S. G. & Balaji, K. N. WNT-inflammasome signaling mediates NOD2-induced development of acute arthritis in mice. *J. Immunol.* **194**, 3351–3360 (2015).
- Spranger, S., Bao, R. & Gajewski, T. F. Melanoma-intrinsic β-catenin signalling prevents anti-tumour immunity. *Nature* **523**, 231–235 (2015).
- Augustinova, A. et al. Tumour cell-derived Wnt7a recruits and activates fibroblasts to promote tumour aggressiveness. *Nat. Commun.* **7**, 10305 (2016).
- Luke, J. J., Bao, R., Sweis, R. F., Spranger, S. & Gajewski, T. F. WNT/β-catenin pathway activation correlates with immune exclusion across human cancers. *Clin. Cancer Res.* **25**, 3074–3083 (2019).
- Kim, N. H. et al. p53 and microRNA-34 are suppressors of canonical Wnt signaling. *Sci. Signal.* **4**, ra71 (2011).
- Nusse, R. & Clevers, H. Wnt/β-catenin signaling, disease, and emerging therapeutic modalities. *Cell* **169**, 985–999 (2017).
- Wellenstein, M. D. & de Visser, K. E. Cancer-cell-intrinsic mechanisms shaping the tumor immune landscape. *Immunity* **48**, 399–416 (2018).

Publisher's note: Springer Nature remains neutral with regard to jurisdictional claims in published maps and institutional affiliations.

METHODS

Mice. All animal experiments were approved by the Animal Ethics Committee of the Netherlands Cancer Institute and performed in accordance with institutional, national and European guidelines for Animal Care and Use. The generation and characterization of the mouse models has been described^{27–34} (and unpublished observations). The following mouse models were used in this study: keratin 14 (*Krt14* or *K14*)-cre; *Cdh1*^{F/F}; *Trp53*^{F/F}, *K14-cre;Trp53*^{F/F}, *K14-cre;Brcal*^{E/F}; *Trp53*^{F/F}, whey acidic protein (*Wap*)-cre; *Trp53*^{F/F}, *Wap-cre;Brcal*^{E/F}; *Trp53*^{F/F}, *Wap-cre;Brcal*^{E/F}; *Trp53*^{F/F}; *Col1a1*^{invCAG-Met-ires-Luc/+} (*Wap-cre;Brcal*^{E/F}; *Trp53*^{F/F}; *Met*), *Wap-cre;Brcal*^{E/F}; *Trp53*^{F/F}; *Col1a1*^{invCAG-Myc-ires-Luc/+} (*Wap-cre;Brcal*^{E/F}; *Trp53*^{F/F}; *Myc*), *Wap-cre;Brcal*^{E/F}; *Trp53*^{F/F}; *Col1a1*^{invCAG-Myb2-ires-Luc/+} (*Wap-cre;Brcal*^{E/F}; *Trp53*^{F/F}; *Myb2*), *Wap-cre;Trp53*^{F/F}; *Col1a1*^{invCAG-ESR1-ires-Luc/+} (*Wap-cre;Trp53*^{F/F}; *HA-ESR1*), *Wap-cre;Cdh1*^{E/F}; *Col1a1*^{invCAG-Akt1E17K-ires-Luc/+} (*Wap-cre;Cdh1*^{E/F}; *Akt1*^{E17K}), *Wap-cre;Cdh1*^{E/F}; *Col1a1*^{invCAG-Pik3caE545K-ires-Luc/+} (*Wap-cre;Cdh1*^{E/F}; *Pik3ca*^{E545K}), *Wap-cre;Cdh1*^{E/F}; *Col1a1*^{invCAG-Fgr2ex1-15-ires-Luc/+} (*Wap-cre;Cdh1*^{E/F}; *Fgr2*^{ex1-15}), *Wap-cre;Cdh1*^{E/F}; *Col1a1*^{invCAG-Fgr2ex1-15-ires-Luc/+} (*Wap-cre;Cdh1*^{E/F}; *Fgr2*^{ex1-15}), *Wap-cre;Cdh1*^{E/F}; *T2/Onc;Rosa26*^{Lox66SBlx71/+} (*Wap-cre;Cdh1*^{E/F}; *SB*), *Wap-cre;Map3k1*^{F/F}; *Pten*^{F/F}, mouse mammary tumour virus LTR (*MMTV*)-*NeuT*. All mouse models were on FVB/N background, except *MMTV-NeuT* and *Wap-cre;Cdh1*^{F/F}; *SB*, which were on BALB/c and a mixed genetic (C57BL/6) and FVB/N) background, respectively. Female mice were monitored twice weekly for the onset of spontaneous mammary tumour formation by palpation starting at 6–7 weeks of age. The perpendicular tumour diameters of mammary tumours were measured twice per week using a calliper, and tumour volume was calculated using volume (mm³) = 0.5(length × width²). Maximum permitted tumour volumes were 1,500 mm³. Age-matched wild-type littermates were used as controls. Average systemic total and cKIT⁺ neutrophil levels in non-tumour-bearing FVB/N and BALB/c mice were similar (data not shown). For orthotopic transplantation experiments, 1 × 10⁶ cells were injected into the right fourth mammary fat pad of wild-type FVB/N mice (Janvier Labs). For intervention studies targeting porcupine, *K14-cre;Cdh1*^{F/F}; *Trp53*^{F/F} mice were treated daily with LGK974³⁵ (10 mg kg⁻¹, in 10% DMSO, 10% cremophor in PBS) or vehicle (10% DMSO, 10% cremophor in PBS) via oral gavage, starting at matched tumour sizes indicated in the figures. For metastasis experiments, the KEP-based model for spontaneous breast cancer metastasis was used as previously described³⁶. In brief, tumour fragments of *K14-cre;Cdh1*^{F/F}; *Trp53*^{F/F} mice were orthotopically transplanted into FVB/N mice and surgically removed when tumours reached 500 mm³ in size. In this model, LGK974 treatment was initiated when tumours were 30–40 mm³ in size and continued until mastectomy, after which mice were monitored for signs of metastatic disease. Disease end point was defined as mice showing signs of respiratory distress or palpable metastatic nodules in lymph nodes or other organs reaching 1,500 mm³ in size. For metastasis experiments using the *Wap-cre;Cdh1*^{E/F}; *Pik3ca*^{E545K} model, matched *Trp53*^{+/-} and *Trp53*^{-/-} tumour-derived cell lines were orthotopically injected in the mammary fat pad of FVB/N mice (1 × 10⁶ cells) and tumours were allowed to grow out until end stage (1,500 mm³). During this time, tumours spontaneously metastasize to the lungs. LGK974 or vehicle treatment was initiated when tumours were 30–40 mm³ and continued until end stage. Orthotopically transplanted *Wap-cre;Cdh1*^{E/F}; *Akt1*^{E17K} tumours did not spontaneously metastasize before the primary tumours reached 1,500 mm³, and surgical removal of the primary tumours was hampered by their highly invasive growth. For intervention studies, mice were randomly distributed over the two treatment arms when tumours reached the indicated size. Tumour measurements and post-mortem analyses were performed in a blinded fashion. Mice were kept in individually ventilated cages, and food and water were provided ad libitum. The maximal permitted disease end points were not exceeded in any of the experiments.

Flow cytometry. Flow cytometry analysis was performed as previously described⁵. In brief, tissues were collected in ice-cold PBS and blood was collected in tubes containing heparin. Tumours and lungs were mechanically chopped using a McIlwain tissue chopper (Mickle Laboratory Engineering). Tumours were digested for 1 h at 37 °C in 3 mg ml⁻¹ collagenase type A (Roche) and 25 µg ml⁻¹ DNase (Sigma) in serum-free DMEM medium. Lungs were digested for 30 min at 37 °C in 100 µg ml⁻¹ Liberase TM (Roche). Enzyme reactions were stopped by addition of cold DMEM, 8% fetal calf serum (FCS) and suspensions were dispersed through a 70-µm cell strainer. Bone marrow was collected from the tibia and femurs of both hind legs and flushed using RPMI, 8% FCS through a 70-µm cell strainer. Single-cell suspensions were treated with NH₄Cl erythrocyte lysis buffer. Before staining, cell suspensions were subjected to Fc receptor blocking (rat anti-mouse CD16/32, BD Biosciences) for 15 min at 4 °C, except for bone marrow (to allow assessment of CD16/32 expression). Cells were stained with conjugated antibodies for 30 min at 4 °C in the dark in 0.5% BSA in PBS. 7AAD (1:20; eBioscience/ThermoFisher) or Fixable Viability Dye eFluor 780 (1:1,000; eBioscience/ThermoFisher) was added to exclude dead cells. For intracellular cytokine staining, single-cell suspensions were stimulated in IMDM containing 8% FCS, 100 IU ml⁻¹ penicillin, 100 mg ml⁻¹ streptomycin, 0.5% β-mercaptoethanol, 50 ng ml⁻¹ PMA, 1 mM ionomycin

and Golgi-Plug (1:1,000; BD Biosciences) for 3 h at 37 °C. Surface antigens were stained first, followed by fixation and permeabilization using the Cytofix/Cytoperm kit (BD Biosciences) and staining of intracellular proteins. All antibodies used are listed in Supplementary Table 1. All experiments were performed using a BD LSR II flow cytometer using Diva software or the Beckman Coulter CyAn ADP flow cytometer using Summit software. Data analyses were performed using FlowJo Software version 9.9.

Cell culture. Mouse cell lines were generated as follows: *Wap-cre;Cdh1*^{E/F}; *Akt1*^{E17K} (WEA) and *Wap-cre;Cdh1*^{F/F}; *Pik3ca*^{E545K} (WEP) tumour material was collected in ice-cold PBS and mechanically chopped using a McIlwain tissue chopper (Mickle Laboratory Engineering). Tumours were subsequently digested for 30 min at 37 °C in 3 mg ml⁻¹ collagenase A, 0.1% trypsin and fungizone in DMEM with 2% FCS. Enzyme reactions were stopped by addition of DMEM and 2% FCS and suspensions were dispersed through a 40-µm cell strainer. Cells were initially cultured in DMEM containing 10% FCS, 100 IU ml⁻¹ penicillin, 100 mg ml⁻¹ streptomycin, insulin, EGF and cholera toxin. After establishment, mouse cell lines were cultured in DMEM medium supplemented with 8% FCS, 100 IU ml⁻¹ penicillin, 100 mg ml⁻¹ streptomycin and 2 mM L-glutamine. To ensure relatedness to parental GEMM tumours, polyclonal cells were used at low passage number for all experiments. MCF-7 cells (provided by T.N.S.) were cultured in DMEM medium supplemented with 8% FCS, 100 IU ml⁻¹ penicillin, 100 mg ml⁻¹ streptomycin and 2 mM L-glutamine. All cell lines were routinely tested for mycoplasma contamination and only mycoplasma-negative cells were used. For in vitro culture of BMMDs, bone marrow was aseptically collected by flushing tibia and femurs from euthanized wild-type mice with sterile RPMI and 8% FCS. Bone marrow cells were cultured for 7 days in RPMI medium supplemented with 8% FCS, 100 IU ml⁻¹ penicillin, 100 mg ml⁻¹ streptomycin and 10 ng ml⁻¹ recombinant M-CSF (Peprotech). BMMDs were collected at day 7 and examined for CD11b and F4/80 expression by flow cytometry. Consistent purities of >95% CD11b⁺F4/80⁺ cells were obtained. For in vitro culture of human MDMs, human PBMCs (Sanquin) were enriched by magnetically activated cell sorting (MACS) using CD14 micro-beads (Miltenyi Biotec). CD14⁺ cells were cultured in RPMI medium supplemented with 8% FCS, 100 IU ml⁻¹ penicillin, 100 mg ml⁻¹ streptomycin and 10 ng ml⁻¹ recombinant M-CSF (Peprotech). MDMs were collected at day 7 and examined for CD11b, CD14 and CD68 expression by flow cytometry. Consistent purities of >95% CD11b⁺CD14⁺CD68⁺ cells were obtained. Where indicated, BMMDs and MDMs were exposed to conditioned medium from tumour cell lines, in the presence or absence of LGK974 (1 µM, Selleck Chemicals) for 24 h and harvested for RNA and/or protein isolation. Conditioned medium was obtained by culturing tumour cells at equal confluence in empty DMEM overnight. Cell growth kinetics in vitro were analysed using the IncuCyte System (Essen BioScience).

RNA isolation and qRT-PCR. RNA was isolated using either TRIzol or a Qiagen RNeasy column followed by treatment with DNase I (Invitrogen). RNA quality was confirmed with a 2100 Bioanalyzer from Agilent. RNA was converted to cDNA with an AMV reverse transcriptase using Oligo(dT) primers (Invitrogen). cDNA (20 ng per well) was analysed by SYBR green real-time PCR with 500 nM primers using a LightCycler 480 thermocycler (Roche). *Actb* and/or *Gapdh* were used as reference genes. Primer sequences used for each gene are listed in Supplementary Table 2. Fold change in expression was calculated using $2^{(\Delta Ct_x - \text{average}(\Delta Ct_{\text{control}}))}$.

Protein isolation and western blotting. Protein lysates of cells and tissue were prepared using RIPA buffer (50 mM Tris-HCl, pH 7.4, 150 mM NaCl, 1% NP-40, 0.5% DOC, 0.1% SDS, 2 mM EDTA) complemented with protease and phosphatase inhibitors (Roche) and protein concentration was quantified using the BCA protein assay kit (Pierce). Protein lysate was loaded onto NuPAGE 4–12% Bis-Tris gradient gels (Invitrogen) and transferred onto Trans-Blot Turbo Mini or Midi Nitrocellulose membranes (BioRad) using Trans-Blot Turbo Transfer System (BioRad). Membranes were blocked in 10% Western Blot Blocking Reagent (Roche) or 3% BSA for 1 h at room temperature. Primary antibody incubation was performed overnight at 4 °C. Membranes were washed using TBS and Tween 20 (TBS-T) and subjected to secondary fluorochrome-conjugated antibodies for 1 h at room temperature and protein was detected using the Odyssey CLx imaging system and processed using ImageJ software 1.48v. Antibodies are listed in Supplementary Table 1.

Immunohistochemistry. Immunohistochemical analyses were performed by the Animal Pathology facility at the Netherlands Cancer Institute. Formalin-fixed tissues were processed, sectioned and stained as described³⁶. In brief, tissues were fixed for 24 h in 10% neutral buffered formalin, embedded in paraffin, sectioned at 4 µm and stained with haematoxylin and eosin (H&E) for histopathological evaluation. H&E slides were digitally processed using the Aperio ScanScope (Aperio). For immunohistochemical analysis, 5-µm paraffin sections were cut, deparaffinized and stained. Antibodies and antigen retrieval methods are listed in Supplementary Table 1. Quantitative analysis of cell abundance was performed by counting cells in five high-power (×40) fields of view (FOV) per tissue by two independent researchers. Samples were visualized with a BX43 upright microscope (Olympus)

and images were acquired in bright field using cellSens Entry software (Olympus). To score pulmonary metastasis, single lung sections were stained for cytokeratin-8 and metastatic nodules were counted by two independent researchers. Stained tissue slides were digitally processed using the Aperio ScanScope. Brightness and contrast for representative images were adjusted equally among groups.

Cytokine analyses. Quantification of cytokine and chemokine levels in serum was performed using BD Cytometric Bead Array for CCL2, IL-1 β , IL-17A and G-CSF according to manufacturer's instructions and analysed on a Beckman Coulter CyAn ADP flow cytometer with Summit software. Data analyses were performed using FlowJo Software version 9.9.

CRISPR-Cas9-mediated gene disruption. For knockout of mouse *Trp53*, p53-proficient tumour cell lines were transfected with lentiCRISPR v2 (provided by F. Zhang (Addgene plasmid 52961)³⁷) containing sgRNA targeting exon 4 (sgRNA1: 5'-TCCGAGTGTCAAGGAGCTCCT-3' and sgRNA2: 5'-AGTGAAGCCCTCGAGTCG-3'). For knockout of human *TP53*, MCF-7 tumour cell lines were transfected with lentiCRISPRv2 containing sgRNA targeting either exon 4 (sgRNA1: 5'-CCATTGTTCAATATCGTCCG-3') or exon 2 (sgRNA2: 5'-TCGACGCTAGGATCTGACTG-3'). Cloning of sgRNAs in lentiCRISPR was performed as described³⁷ and sgRNA sequences were designed using the online CRISPR Design tool (<http://crispr.mit.edu>), of which the two highest scoring sequences were chosen. All vectors were validated by Sanger sequencing. After selection of transfected cells, polyclonal cell lines were used for all subsequent experiments. To determine knockout efficiency, genomic DNA from cell lines was isolated using Viagen DirectPCR Lysis reagent (Cell) supplemented with 200 μ g ml⁻¹ proteinase K after transfection and puromycin selection. The mouse *Trp53* target region was amplified using PCR with the following primers: forward 5'-GGGGACTGCAGGGTCTCAGA-3' and reverse 5'-CCACGTCCCCTGGAGAGATG-3'. The human *TP53* target region was amplified using PCR with the following primers: FW1 5'-CAGACTG CCTTCCGGGTAC-3' for sgRNA1, FW2 5'-TGGGAAGGTTGGAAGT CCCTC-3' for sgRNA2, and RV 5'-CACTGACAGGAAGCCAAGGG-3'. PCR products were run on 1% agarose gel, purified using the Illustra GFX PCR DNA and Gel Band Purification Kit (Sigma), and subjected to Sanger sequencing using their respective forward primers. Genome editing efficiency was quantified using the Tracking of Indels by Decomposition (TIDE) algorithm as described (<http://tide.nki.nl>)³⁸.

shRNA- and siRNA-mediated knockdown of genes. Vectors for shRNAs were collected from the TRC library. To allow stable expression of shRNAs, HEK293T cells (provided by T.N.S.) were transfected with the pLKO.1 lentiviral vector encoding shRNAs, pPAX packaging vector and VSV-G envelope vector. Five independent shRNA clones were used for each experiment. Virus was collected at day 4 and 5 and viral titres were determined using the Abm qPCR lentivirus titration kit (LV900). Cell lines were subsequently transduced and selected using puromycin. Knockdown efficiency was determined by RT-qPCR compared to non-targeting controls. The shRNA clone used for *Porcn* knockdown in all experiments after assessment of knockdown efficiency contained following hairpin sequence: 5'-CAACTTCTATGCCTGTCAT-3' (shPorcn-1) or 5'-CCCATGCTTATTGGTTAAAT-3' (shPorcn-4). For *in vivo* experiments, shPorcn-4 was used. To silence *Fzd* receptors, BMDMs were transfected with the following siRNA pools (control siRNA (sc-37007), *Fzd7* (sc-39991) and *Fzd9* (sc-39995), Santa Cruz Biotechnology), according to the manufacturer's instructions. In brief, BMDMs were differentiated as described above, and 24 h before exposure to tumour conditioned medium and BMDMs were suspended in transfection medium and incubated with indicated siRNA pools. After 6 h at 37 °C, 2 × RPMI medium was added (RPMI, 20% serum, 200 IU ml⁻¹ penicillin, 200 mg ml⁻¹ streptomycin and 20 ng ml⁻¹ recombinant M-CSF) and BMDMs were further cultured overnight. After 24 h, the medium was replaced by tumour conditioned medium for 24 h, after which gene expression was assessed.

ChIP-seq analysis. ChIP-seq analysis was performed as previously described³⁹. In brief, cell lines from *Wap-cre;Cdh1^{E1/F};Akt1^{E1/K}* and *Wap-cre;Cdh1^{E1/F};Pik3ca^{E545K}* tumours (3 cell lines from 3 independent mouse tumours per genotype) were fixed in 1% formaldehyde, crosslinked and processed for sonication. Subsequently, 5 μ g of p53 antibody (Supplementary Table 1) and 50 μ l of protein G magnetic beads (Invitrogen) were used for each ChIP. Eluted DNA was sequenced using the Illumina Hiseq 2500 analyser (using 65 bp reads) and aligned to the *Mus musculus* mm10 reference genome. Peak calling over input control was performed using and MACS 2.0 peak caller. Data were visualized using Eased⁴⁰.

Overexpression of miR-34a. The MSCV-miR-34a retroviral vector (provided by L. He (Addgene plasmid 63932)⁴¹) was transfected in HEK293T cells, together with pGag-Pol and VSV-G vectors to generate retrovirus. Mouse cancer cell lines were exposed to viral supernatant and assessed for expression of WNT target genes after puromycin selection.

RNA sequencing and analysis. Total RNA was extracted from tumours using TRIzol reagent (Ambion Life Technologies) according to the manufacturer's

instructions. Samples were equimolar pooled and were single-end sequenced for 51 or 65 base pairs on the Illumina Hiseq2000/Hiseq2500 Machine. The reads were aligned against the mouse transcriptome (mm10) using Tophat2 (Tophat version 2.1.0, Bowtie version 1.0.0) that allows for exon-exon junctions^{42,43}. Tophat was guided using a reference genome as well as a reference transcriptome. The reference transcriptome was created using a gene transfer file (GTF) that was downloaded from Ensembl (v.77). Gene counts were generated using a custom script that functions identically to HTSeq-count⁴⁴. Only reads that mapped uniquely to the transcriptome were used for gene expression quantification. Although some of the libraries were generated with strand-specific protocols, all samples have been aligned without taking strandedness into account. Next, differential expression analysis was performed using the R package edgeR⁴⁵ in combination with the voom⁴⁶ method, using raw read counts as input. Library size normalization was performed during differential expression analysis within the voom function. Genes with $P < 0.05$ were labelled as differentially expressed. Genes were further filtered for display by requiring them to be protein coding and to have an absolute log₂-transformed fold change ≥ 3 and a $P \leq 0.01$. The selected genes were shown in a heat map of read counts that were normalized to 10 million reads per sample.

For Hallmark pathway analysis of mouse transcriptomes, raw read counts were normalized by trimmed means of M-values computed using the function calcNormFactors (edgeR v.3.20.5⁴⁵), from which counts per million (CPM)-normalized gene expression values were computed for plotting purposes using the same R package. CPM values were subsequently transformed as $f(x) = \log_2(x + 1)$. Ensembl77 mouse gene identifiers were then converted to homologous human gene identifiers using the biomaRt R package (server oct2016.archive.ensembl.org). Gene expression heat maps for hallmark human gene sets obtained from MsigDB⁴⁷ were generated using the 'heatmap' function provided by the NMF R package (version 0.20.6). Heat map columns (containing samples) were ordered according to average linkage (UPGMA) hierarchical sample clustering based on Pearson correlation distances between the expression values of displayed genes. Heat map rows (containing genes) were ordered according to gene expression fold difference between *Trp53*^{-/-} and *Trp53*^{+/+} samples. The R language for statistical computing was used (v.3.4.2) for gene expression normalization and heat map generation. Pathway enrichment analysis of *Trp53*^{-/-} and *Trp53*^{+/+} tumours was performed using Ingenuity Pathway Analysis software (QIAGEN), analysing differentially expressed genes with $P \leq 0.05$.

TCGA analysis. To obtain a comprehensive view on the cellular processes affected by p53 deficiency in human breast cancer, we performed a gene set enrichment analysis (GSEA) using a 50 hallmark gene sets (Liberzon)⁴⁷ on the TCGA breast cancer (BRCA) cohort. First, we classified p53 deficiency based on mutational status. DNA sequencing variant calls (MAF-file) for the BRCA cohort were downloaded from the 21 August 2015 release of the Broad TCGA genome data analysis centre standard run (<http://gdac.broadinstitute.org/runs/stddata>). We used two classifications for p53 deficiency: in the first classification (labelled 'any *TP53* mutation'), patients with any kind of *TP53* mutation were classified as p53 deficient. In the second classification (labelled 'IARC *TP53* database'), only patients with a dominant-negative *TP53* mutation as annotated using the IARC *TP53* mutation database⁴⁸ (release 18, matched on protein effect of the mutation) were labelled as p53 deficient, as well as patients with gain-of-stop, stop-lost or frameshifting mutations ($n = 161$). One sample had a trans-activating mutation and was excluded from the analysis. The remaining samples were labelled as p53 proficient ($n = 793$).

Next, TCGA RNA sequencing data were downloaded from the Broad TCGA genome data analysis centre 1 November 2015 release of the standard runs. We ran a GSEA on the 50 Hallmark gene set using the flexgsea-r R package (<https://github.com/NKI-CCB/flexgsea-r>) on the read counts normalized with limma voom with the span parameter set to 0.5⁴⁶. Within each permutation of the sample labels, genes were ranked for association with p53 proficiency using the moderated *t*-statistic from the limma empirical Bayes function (ebayes()) ran on the result of lmFit(). Reported FDR-values were obtained from the flexgsea-r output.

Single gene associations with *TP53* status in human breast tumours of the TCGA BRCA cohort and correlation coefficients between WNT-related genes and *TP53* status (mutant versus wild type) were analysed using R2 Genomics Analysis and Visualization Platform (<http://r2.amc.nl/>) and visualized using GraphPad Prism version 7.

Statistics and reproducibility. Data analyses were performed using GraphPad Prism (version 7). The statistical tests used are described in figure legends. All tests were performed two-tailed. $P < 0.05$ was considered statistically significant. All western blot and RT-qPCR analyses were independently repeated more than twice. Sample sizes were based on previous experiments^{5,17,36} or determined using G*Power software (version 3.1). To exclude bias towards one particular GEMM in the analyses for Fig. 1, we have performed the same analyses on the average of the neutrophil levels and serum cytokine values per model. This demonstrated the same correlations between the assessed values and p53 status of the tumour, thus excluding bias towards one or several particular models. Principal

component analysis was performed using the prcomp-function in R (version 3.4.2), both centering and scaling the input data before applying dimensionality reduction. **Reporting summary.** Further information on research design is available in the Nature Research Reporting Summary linked to this paper.

Data availability

The RNA-seqencing data have been deposited in the Gene Expression Omnibus (GEO, NCBI) repository under accession number GSE112665. All other data are found in the Source Data, Supplementary Information or available from the authors on reasonable request.

27. Boggio, K. et al. Interleukin 12-mediated prevention of spontaneous mammary adenocarcinomas in two lines of Her-2/neu transgenic mice. *J. Exp. Med.* **188**, 589–596 (1998).
28. Jonkers, J. et al. Synergistic tumor suppressor activity of BRCA2 and p53 in a conditional mouse model for breast cancer. *Nat. Genet.* **29**, 418–425 (2001).
29. Derkzen, P. W. et al. Somatic inactivation of E-cadherin and p53 in mice leads to metastatic lobular mammary carcinoma through induction of anoikis resistance and angiogenesis. *Cancer Cell* **10**, 437–449 (2006).
30. Liu, X. et al. Somatic loss of BRCA1 and p53 in mice induces mammary tumors with features of human BRCA1-mutated basal-like breast cancer. *Proc. Natl Acad. Sci. USA* **104**, 12111–12116 (2007).
31. Henneman, L. et al. Selective resistance to the PARP inhibitor olaparib in a mouse model for BRCA1-deficient metaplastic breast cancer. *Proc. Natl Acad. Sci. USA* **112**, 8409–8414 (2015).
32. Huijbers, I. J. et al. Using the GEMM-ESC strategy to study gene function in mouse models. *Nat. Protocols* **10**, 1755–1785 (2015).
33. Kas, S. M. et al. Insertional mutagenesis identifies drivers of a novel oncogenic pathway in invasive lobular breast carcinoma. *Nat. Genet.* **49**, 1219–1230 (2017).
34. Annunziato, S. et al. Comparative oncogenomics identifies combinations of driver genes and drug targets in BRCA1-mutated breast cancer. *Nat. Commun.* **10**, 397 (2019).
35. Liu, J. et al. Targeting Wnt-driven cancer through the inhibition of Porcupine by LGK974. *Proc. Natl Acad. Sci. USA* **110**, 20224–20229 (2013).
36. Doornbehal, C. W. et al. A preclinical mouse model of invasive lobular breast cancer metastasis. *Cancer Res.* **73**, 353–363 (2013).
37. Sanjana, N. E., Shalem, O. & Zhang, F. Improved vectors and genome-wide libraries for CRISPR screening. *Nat. Methods* **11**, 783–784 (2014).
38. Brinkman, E. K., Chen, T., Amendola, M. & van Steensel, B. Easy quantitative assessment of genome editing by sequence trace decomposition. *Nucleic Acids Res.* **42**, e168 (2014).
39. Schmidt, D. et al. ChIP-seq: using high-throughput sequencing to discover protein-DNA interactions. *Methods* **48**, 240–248 (2009).
40. Lerdrup, M., Johansen, J. V., Agrawal-Singh, S. & Hansen, K. An interactive environment for agile analysis and visualization of ChIP-sequencing data. *Nat. Struct. Mol. Biol.* **23**, 349–357 (2016).
41. Okada, N. et al. A positive feedback between p53 and miR-34 miRNAs mediates tumor suppression. *Genes Dev.* **28**, 438–450 (2014).
42. Kim, D. et al. TopHat2: accurate alignment of transcriptomes in the presence of insertions, deletions and gene fusions. *Genome Biol.* **14**, R36 (2013).
43. Trapnell, C., Pachter, L. & Salzberg, S. L. TopHat: discovering splice junctions with RNA-Seq. *Bioinformatics* **25**, 1105–1111 (2009).
44. Anders, S., Pyl, P. T. & Huber, W. HTSeq—a Python framework to work with high-throughput sequencing data. *Bioinformatics* **31**, 166–169 (2015).
45. Robinson, M. D., McCarthy, D. J. & Smyth, G. K. edgeR: a Bioconductor package for differential expression analysis of digital gene expression data. *Bioinformatics* **26**, 139–140 (2010).
46. Law, C. W., Chen, Y., Shi, W. & Smyth, G. K. voom: precision weights unlock linear model analysis tools for RNA-seq read counts. *Genome Biol.* **15**, R29 (2014).
47. Liberzon, A. et al. The Molecular Signatures Database (MSigDB) hallmark gene set collection. *Cell Syst.* **1**, 417–425 (2015).
48. Bouaoun, L. et al. TP53 variations in human cancers: new lessons from the IARC TP53 database and genomics data. *Hum. Mutat.* **37**, 865–876 (2016).

Acknowledgements Research in the De Visser laboratory is funded by a European Research Council Consolidator award (ERC InflaMet 615300), the Netherlands Organization for Scientific Research (NWO-VICI 91819616), Oncode Institute, the Dutch Cancer Society (KWF10083; KWF10623) and the Beug Foundation for Metastasis Research. K.E.d.V. is an EMBO Young Investigator. Research in the Jonkers laboratory is funded by ERC Synergy grant 319661. We thank members of the De Visser and Jonkers laboratories and R. Mezzadra for fruitful discussion during the preparation of the manuscript. We thank O. van Tellingen, the Mouse Clinic for Cancer and Aging (MCCA) intervention Unit, flow cytometry facility, mouse transgenic facility, genomics core facility, animal laboratory facility and animal pathology facility of the Netherlands Cancer Institute for technical assistance.

Author contributions M.D.W., S.B.C., J.J. and K.E.d.V. conceived the ideas and designed the experiments. M.D.W., S.B.C., D.E.M.D. and M.H.v.M. performed the animal experiments, flow cytometry, RT-qPCR, serum analyses, western blot, immunohistochemistry and other experiments and analysed the data. C.-S.H., K.V., A.P.D., E.S. and R.d.K.-G. provided technical support and performed animal experiments. M.H.v.M., L.H., S.M.K. and J.J. generated mouse models. M.D.W. and R.d.K.-G. performed mouse intervention experiments. I.v.d.H. generated the GEMM-derived cell lines. S.P., M.D.W. and W.Z. performed and analysed the ChIP-seq experiments. M.S., I.d.R., M.D.W., L.F.A.W. and T.N.S. performed the bioinformatics analyses on mouse and human RNA-sequencing datasets. M.D.W., S.B.C. and K.E.d.V. wrote the paper and prepared the figures, with input from all authors.

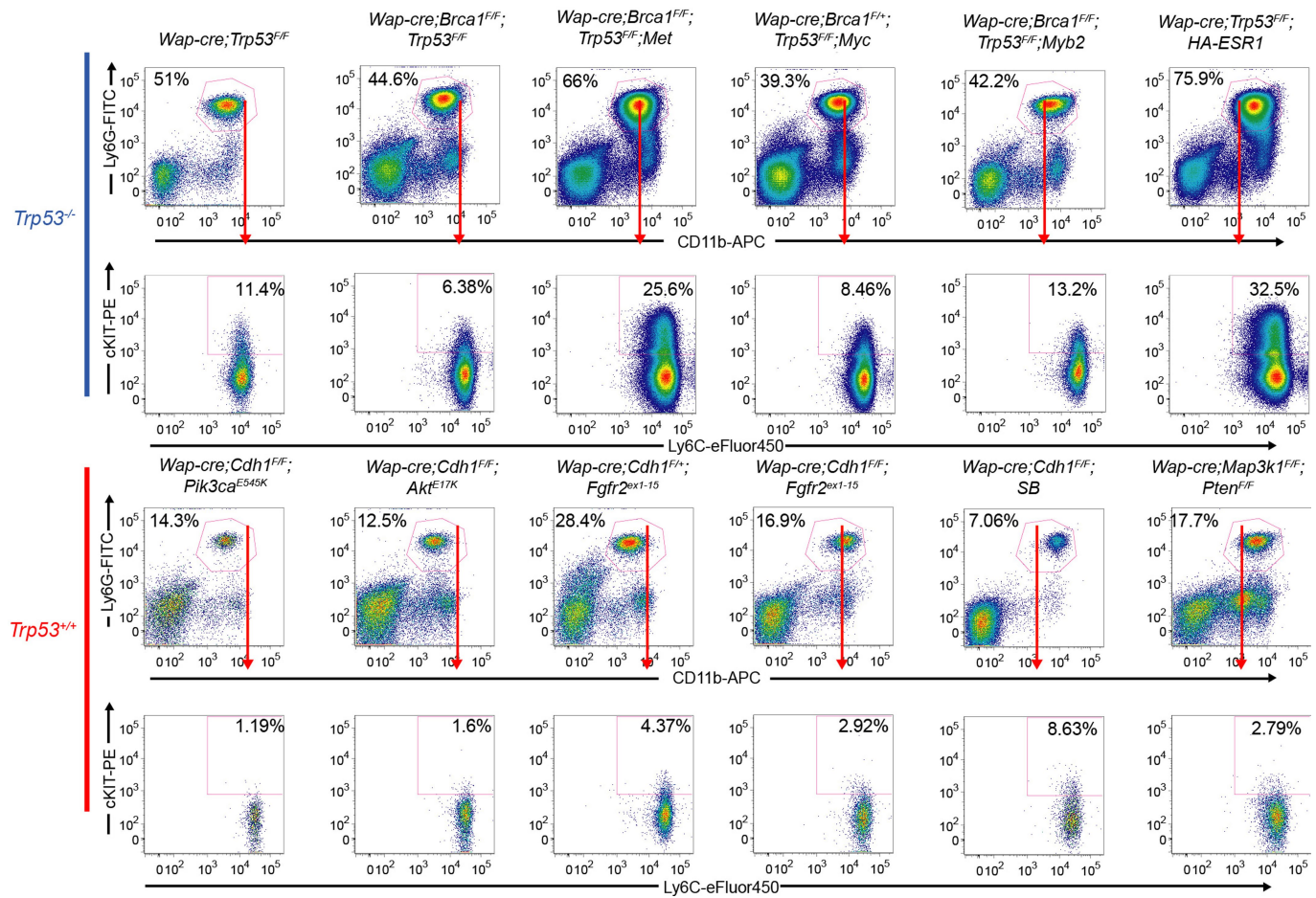
Competing interests M.D.W., S.B.C., D.E.M.D., M.H.v.M., M.S., I.d.R., L.H., S.M.K., S.P., C.-S.H., K.V., A.P.D., R.d.K.-G., E.S., I.v.d.H., W.Z. and J.J. report no competing interests. L.F.A.W. reports research funding from Genmab. T.N.S. is a consultant for Adaptive Biotechnologies, AIMM Therapeutics, Allogene Therapeutics, Amgen, Merus, Neon Therapeutics, Scenic Biotech and Third Rock Ventures, reports research support from Merck, Bristol-Myers Squibb, Merck KGaA, and is stockholder in AIMM Therapeutics, Allogene Therapeutics, Merus, Neogene Therapeutics, Neon Therapeutics and Scenic Biotech, all outside the scope of this work. K.E.d.V. reports research funding from Roche and is consultant for Third Rock Ventures, outside the scope of this work.

Additional information

Supplementary information is available for this paper at <https://doi.org/10.1038/s41586-019-1450-6>.

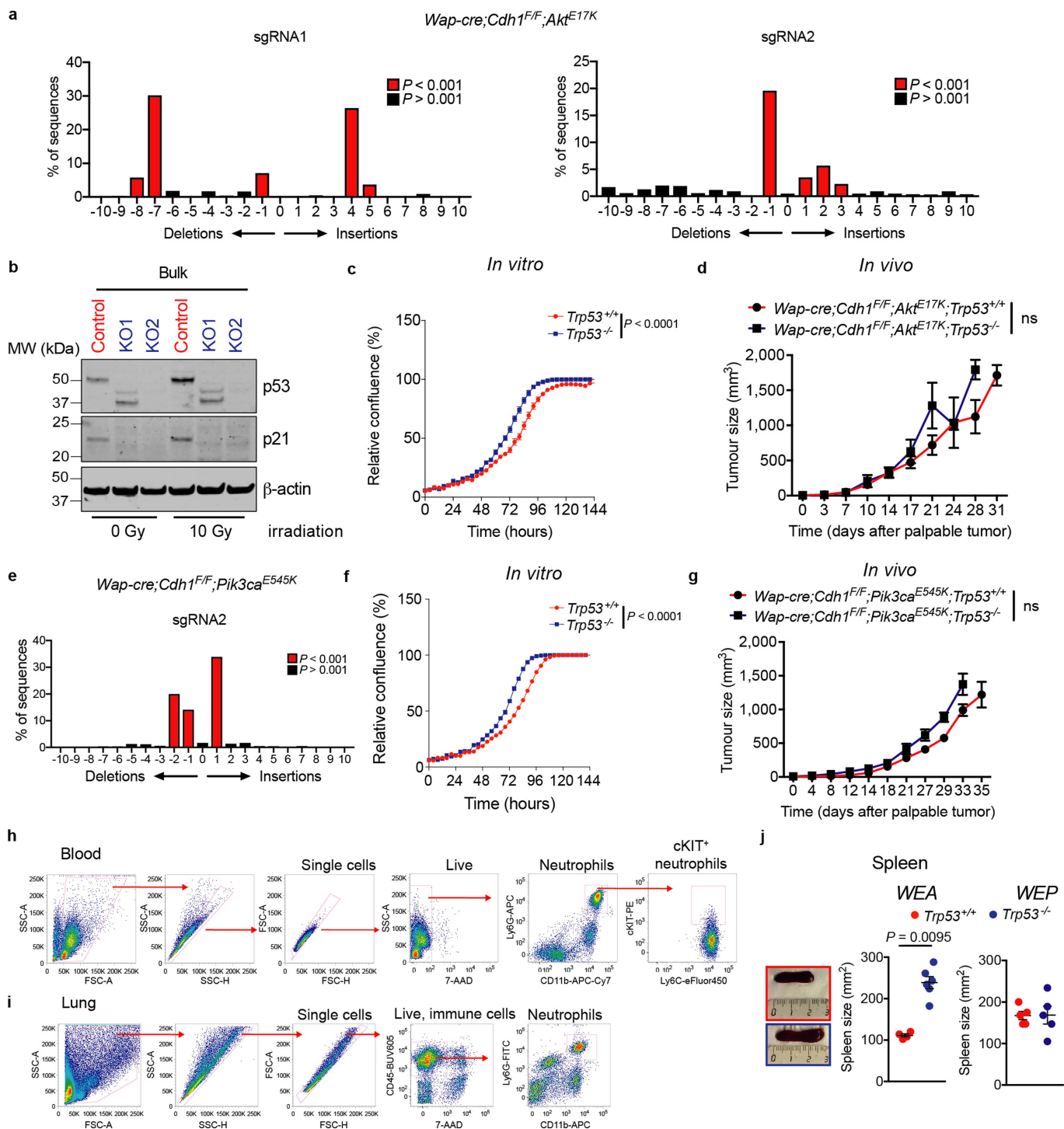
Correspondence and requests for materials should be addressed to J.J. or K.E.d.V.

Reprints and permissions information is available at <http://www.nature.com/reprints>.

a Gated on live cells:

Extended Data Fig. 1 | Neutrophil expansion in p53-deficient tumour-bearing GEMMs. **a**, Representative plots of flow cytometry analysis on blood of end-stage (cumulative tumour size $1,500 \text{ mm}^3$) mammary tumour-bearing mice. Neutrophils were defined as $\text{CD11b}^+ \text{Ly6G}^+ \text{Ly6C}^-$.

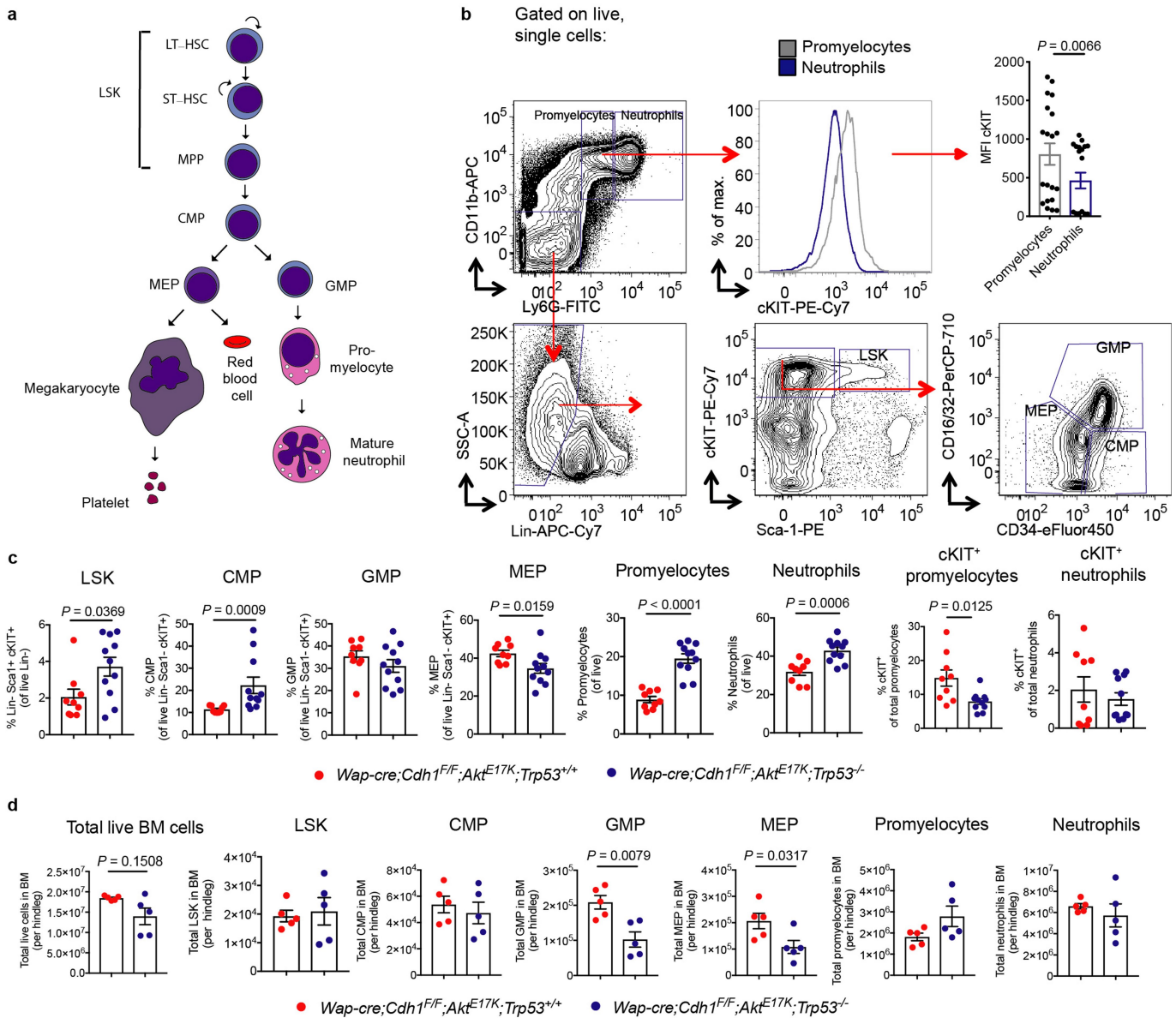
cKIT expression on gated total neutrophils in blood is shown (gating was based on blood of wild-type mice). Quantification and statistical analysis of these data are found in Fig. 1a, b.



Extended Data Fig. 2 | See next page for caption.

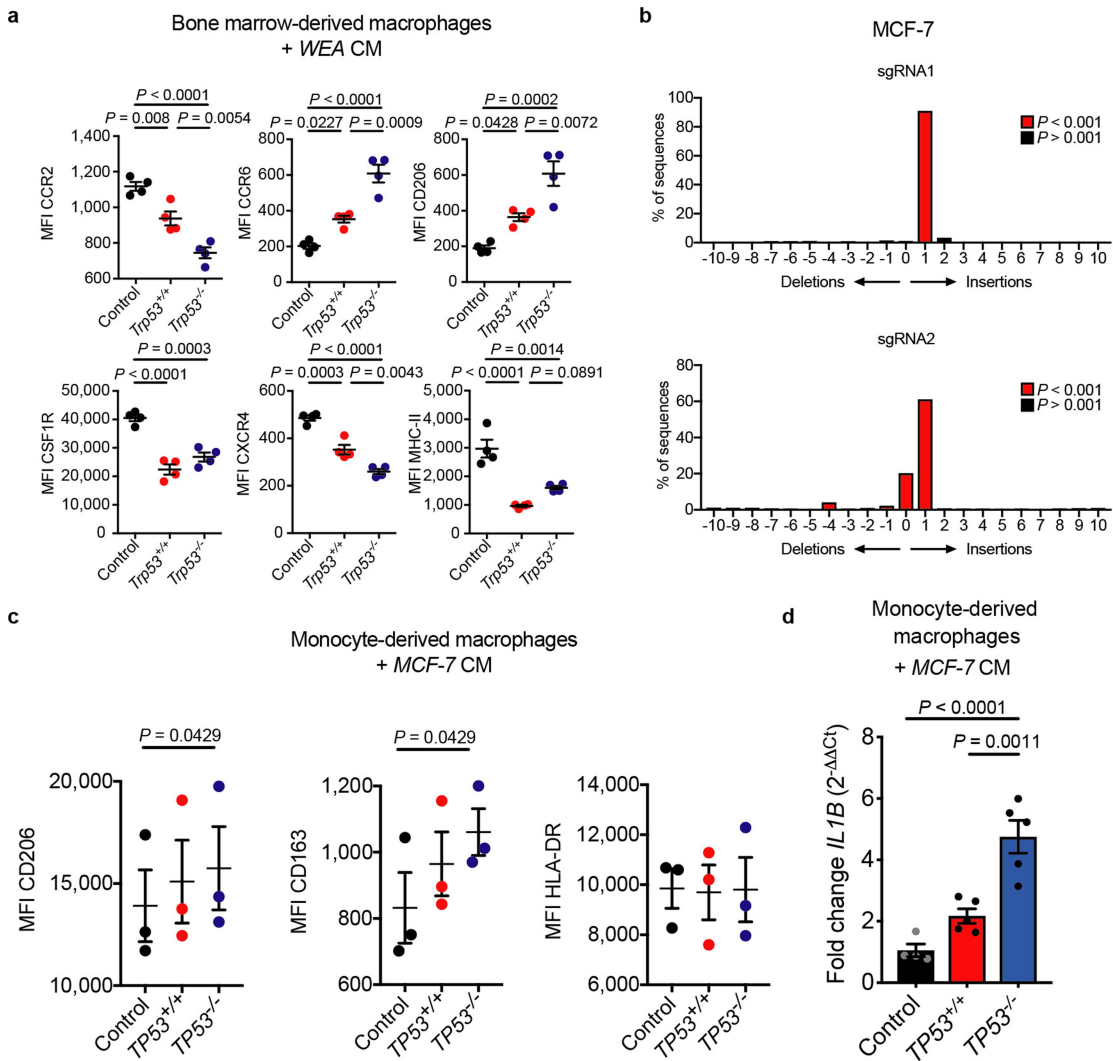
Extended Data Fig. 2 | CRISPR–Cas9-mediated gene disruption of *Trp53* in WEA and WEP cancer cell lines. **a**, Insertion and deletion (indel) spectrum of bulk *Wap-cre;Cdh1^{F/F};Akt1^{E17K}* (WEA) cancer cell lines after transfection with two individual sgRNAs against *Trp53* and puromycin selection, as determined by the TIDE algorithm and compared to the sequence of target region of control cells. *P* values associated with the estimated abundance of each indel are calculated by a two-tailed *t*-test of the variance–covariance matrix of the s.e.m. **b**, Western blot analysis showing p53 levels of control and p53-knockout WEA cell lines. Inactivation of the p53 pathway is shown by loss of p21 staining after 10 Gy irradiation. KO1 (sgRNA1) resulted in a truncated p53 protein, and KO2 (sgRNA2) shows absence of p53 protein. For all subsequent experiments, KO2 was used. Blot is representative of two independent experiments. For uncropped images, see Supplementary Fig. 1. **c**, In vitro growth kinetics of WEA control and p53-knockout cells, as determined by IncuCyte ($n = 7$ technical replicates per group). **d**, In vivo growth kinetics of orthotopically transplanted *WEA;Trp53^{+/+}* ($n = 4$ mice) and *WEA;Trp53^{-/-}* ($n = 6$

cancer cell lines, with $t = 0$ being the first day tumours were palpable. **e**, Indel spectrum of bulk *Wap-cre;Cdh1^{F/F};Pik3ca^{E545K}* (WEP) cancer cell lines after transfection with sgRNA2 against *Trp53* and puromycin selection, as determined by the TIDE algorithm. **f**, In vitro growth kinetics of WEP control and p53-knockout cells, as determined by IncuCyte ($n = 7$ technical replicates per group). **g**, In vivo growth kinetics of orthotopically transplanted *WEP;Trp53^{+/+}* ($n = 5$) and *WEP;Trp53^{-/-}* ($n = 5$) cell lines, with $t = 0$ being the first day tumours were palpable. **h**, Gating strategy to identify circulating neutrophils and their cKIT expression. **i**, Gating strategy to identify neutrophils in the lung. **j**, Representative images of spleens from mice bearing *WEA;Trp53^{+/+}* and *WEA;Trp53^{-/-}* tumours and quantification of spleen area (length \times width) at end stage (tumour volume 1,500 mm 3) of mice bearing p53-proficient ($n = 4$) and p53-deficient WEA ($n = 6$) and WEP ($n = 5$ per group) tumours. All data are mean \pm s.e.m. *P* values were determined by area under the curve (AUC) analysis followed by two-tailed Welch's *t*-test (**c**, **d**, **f**, **g**) or two-tailed Mann–Whitney *U*-test (**j**). ns, not significant.



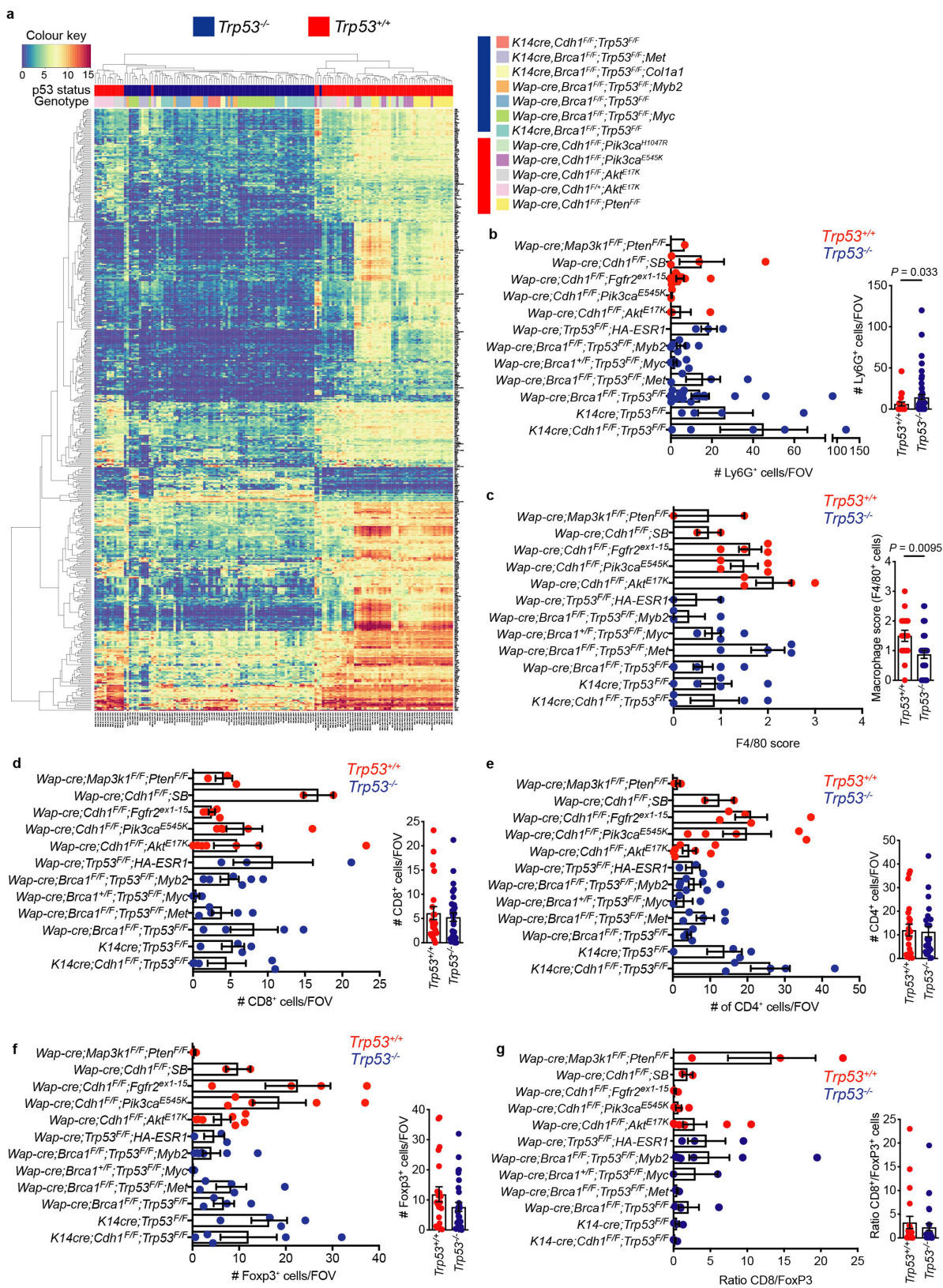
Extended Data Fig. 3 | Haematopoiesis in p53-null tumour-bearing mice is skewed towards the development of neutrophils. **a**, Schematic representation of neutrophil development in the bone marrow. **b**, Gating strategy of neutrophil progenitor populations in the bone marrow. Dot plot indicates the cKIT expression levels in promyelocytes compared with mature neutrophils ($n = 20$ mice). MFI, median fluorescence intensity. **c**, Frequency of bone marrow progenitor populations in mice bearing end-stage *Wap-cre; Cdh1^{F/F}; Akt^{E17K}; Trp53^{+/+}* ($n = 9$) and *Wap-cre; Cdh1^{F/F}; Akt^{E17K}; Trp53^{-/-}* ($n = 11$) tumours, as determined by flow cytometry.

d, Total live cells and total live progenitor population numbers per hindleg of mice bearing *WEA; Trp53^{+/+}* and *WEA; Trp53^{-/-}* tumours ($n = 5$ per group). All data are \pm s.e.m. P values are determined by two-tailed Mann–Whitney U -test. LSK, Lin⁻Sca1⁺cKIT⁺, which contain the LT-HSC (long-term haematopoietic stem cells), ST-HSC (short-term haematopoietic stem cells) and MPP (multipotent progenitors). CMP, common myeloid progenitors; GMP, granulocytic and monocytic progenitors; MEP, megakaryocyte and erythrocyte progenitors.



Extended Data Fig. 4 | Macrophages are differentially activated by *Trp53*^{-/-} mouse and human breast cancer cell lines. **a**, Expression of CCR2, CCR6, CD206, CSF-1R, CXCR4 and MHC-II on live CD11b⁺F4/80⁺ BMDMs after exposure to control medium or conditioned medium (CM) of *Wap-cre;Cdh1*^{E/F}; *Akt1*^{E17K}; *Trp53*^{+/+} or *Wap-cre;Cdh1*^{E/F}; *Akt1*^{E17K}; *Trp53*^{-/-} cell lines, as determined by flow cytometry ($n = 4$ biological replicates per group). **b**, TIDE analysis of bulk MCF-7 cells after transfection with *TP53*-targeting sgRNAs and puromycin selection. For subsequent experiments, sgRNA1 was used. **c**, Expression of CD206, CD163 and HLA-DR on human CD11b⁺CD14⁺CD68⁺ monocyte-derived

macrophages (MDMs) after exposure to conditioned medium of *TP53*^{+/+} MCF-7 or *TP53*^{-/-} (sgRNA1) MCF-7 cancer cells ($n = 3$ biological replicates per group). **d**, RT-qPCR analysis showing *IL1B* expression in human CD11b⁺CD14⁺CD68⁺ MDMs after exposure to control medium ($n = 4$ biological replicates) conditioned medium of *TP53*^{+/+} MCF-7 or *TP53*^{-/-} MCF-7 cancer cells ($n = 5$ biological replicates per group). Data are normalized to normal medium control. Plots are representative of three separate experiments and average of two technical replicates. All data are mean \pm s.e.m. *P* values were determined by two-tailed one-way ANOVA with Tukey's multiple-testing correction.

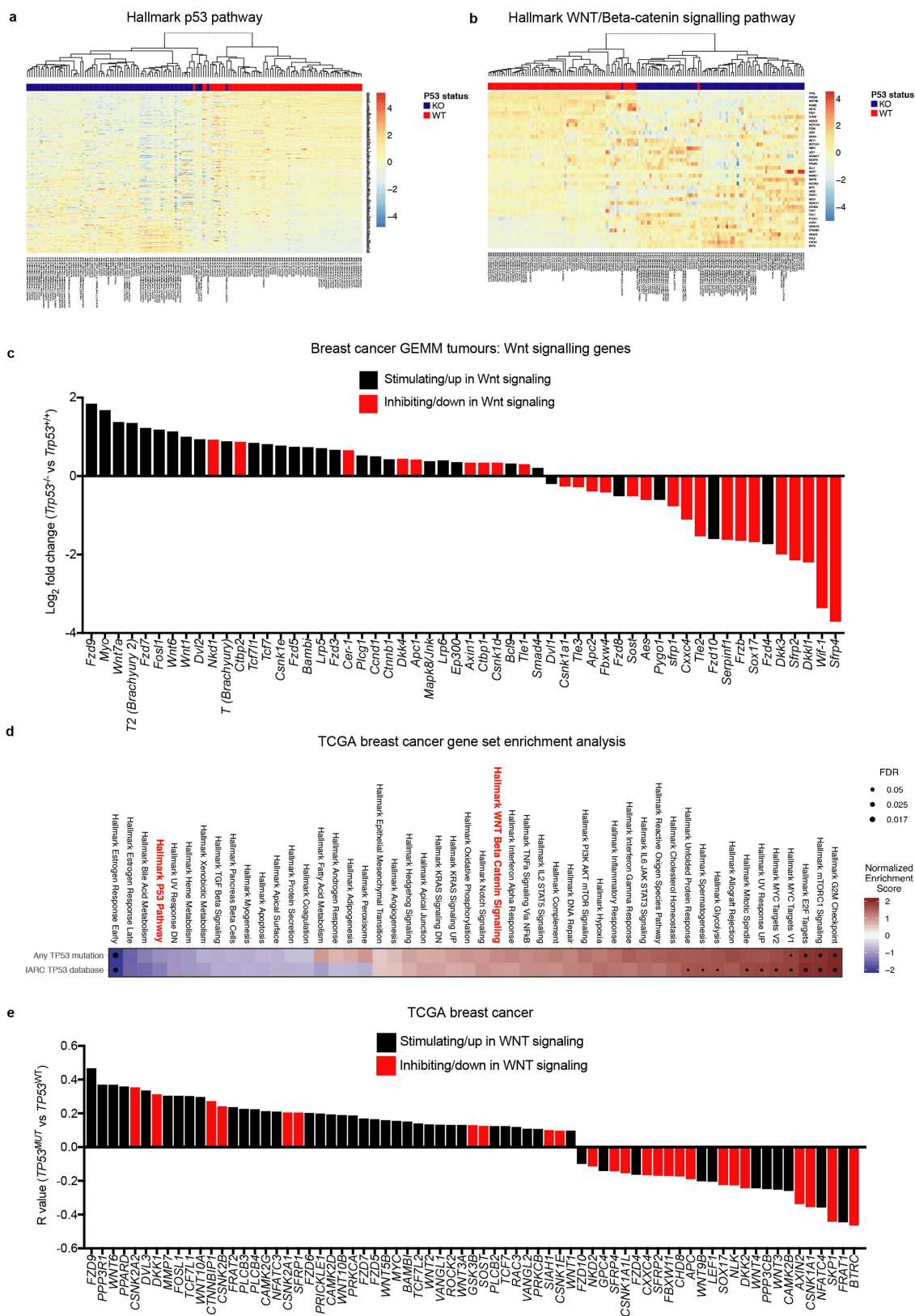


Extended Data Fig. 5 | See next page for caption.

Extended Data Fig. 5 | Transcriptome profile and composition of the local tumour immune landscape in breast cancer GEMMs.

a, Unsupervised clustering of the top 200 most differentially expressed genes ($P < 0.01$, log-transformed fold change >3 or <-3) in mammary GEMM tumours as determined by RNA sequencing ($n = 145$ tumours). Red bars indicate *Trp53^{+/+}* tumours, blue bars indicate *Trp53^{-/-}* tumours. Full tumour genotype is displayed in legend and shown by indicated colours. **b**, Number of Ly6G⁺ neutrophils in the tumour ($n = 1, 4, 10, 2, 4, 3, 6, 13, 4, 22, 4$ and 5 mice, top to bottom). **c**, Macrophage score as indicative of F4/80⁺ macrophage abundance in the tumour ($n = 2, 2, 4, 4, 4, 2, 3, 5, 4, 9, 5$ and 4 mice, top to bottom). **d**, Number of CD8⁺ cytotoxic

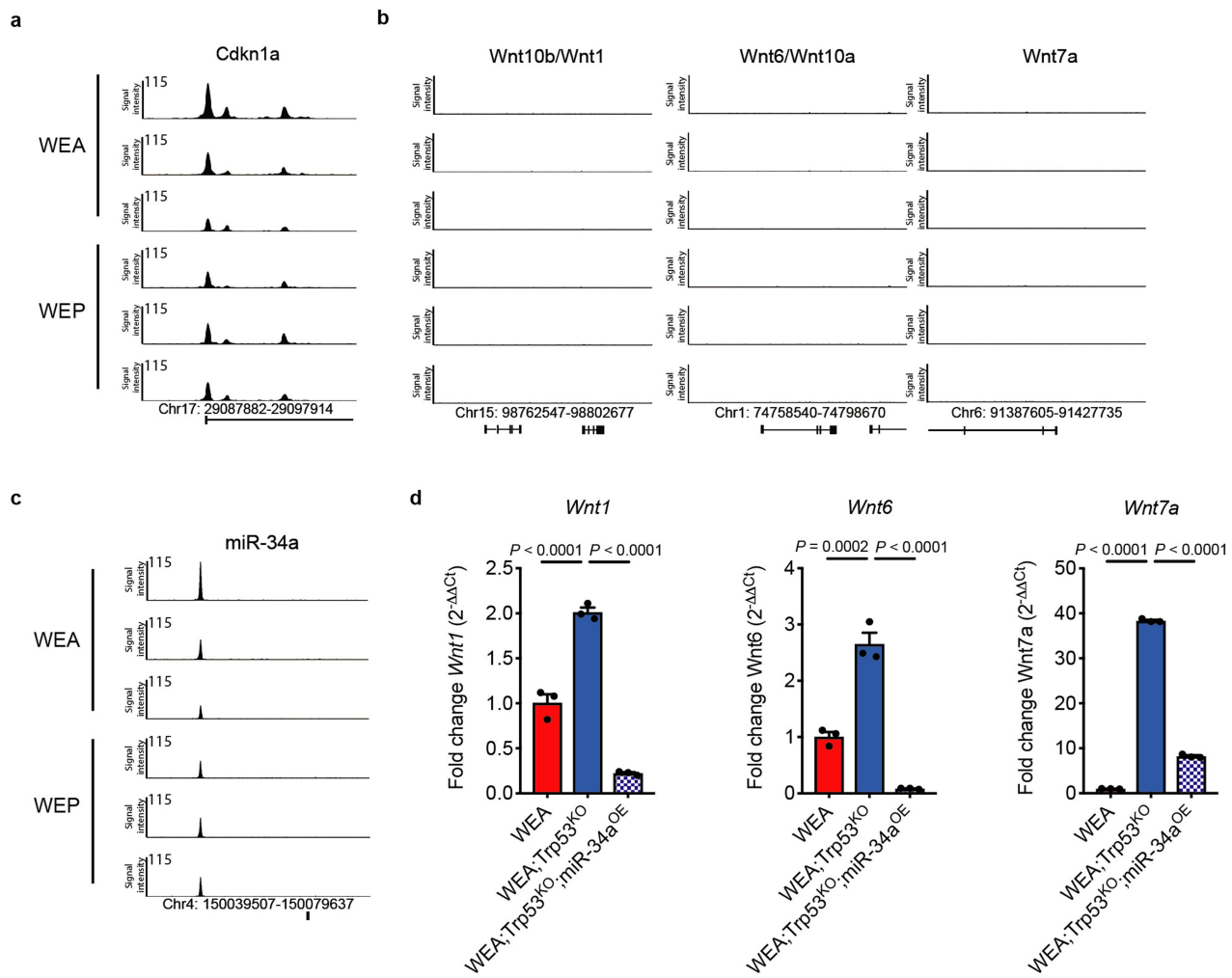
T cells in the tumour ($n = 3, 2, 5, 5, 7, 3, 7, 3, 5, 4, 4$ and 5 mice, top to bottom). **e**, Number of CD4⁺ T cells in the tumour ($n = 3, 2, 5, 5, 7, 3, 7, 3, 5, 4, 4$ and 5 mice, top to bottom). **f**, Number of FOXP3⁺ regulatory T cells in the tumour ($n = 3, 2, 5, 5, 7, 3, 7, 3, 5, 4, 4$ and 5 mice, top to bottom). **g**, Ratio of CD8/FOXP3 cells in the tumour ($n = 3, 2, 5, 5, 7, 3, 7, 2, 5, 4, 4$ and 5 mice, top to bottom). All data are the mean of five microscopic fields of view (FOV) per mouse as determined by immunohistochemistry. Inserts show data combined according to p53 status of the tumour. Each symbol represents an individual mouse. All data are mean \pm s.e.m. P values are determined by two-tailed one-way ANOVA with FDR multiple-testing correction (**a**) or two-tailed Mann–Whitney *U*-test (**b–g**).



Extended Data Fig. 6 | See next page for caption.

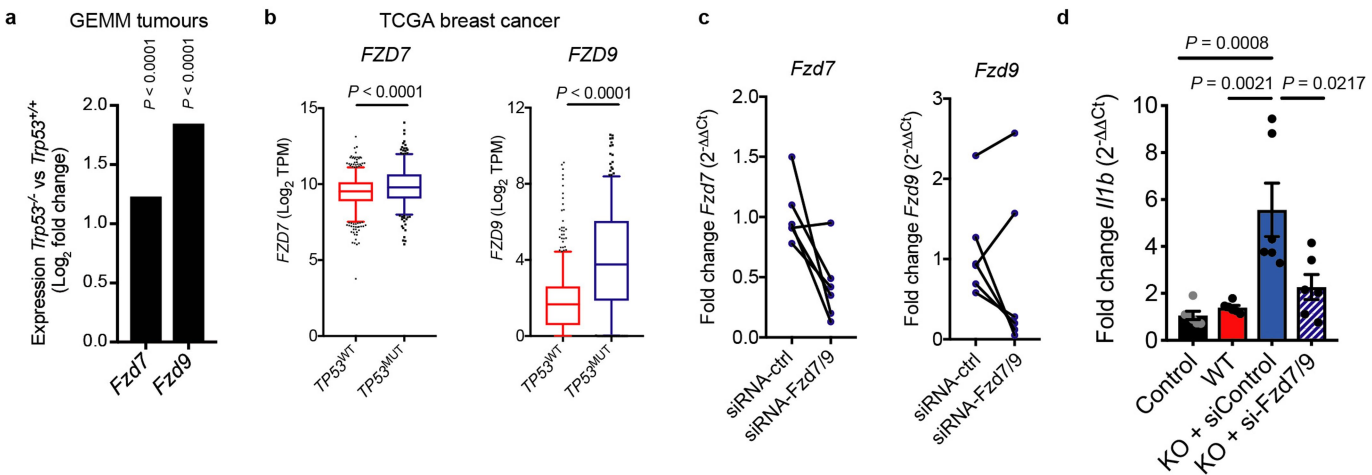
Extended Data Fig. 6 | WNT-related gene activation correlates with loss of p53 in mouse and human breast tumours. **a, b,** Heat maps showing that *Trp53^{-/-}* (KO) GEMM tumours ($n = 77$) cluster away from *Trp53^{+/+}* (WT) tumours ($n = 68$) based on analysis of the Hallmark p53 pathway (represents positive control) (**a**) and analysis of the Hallmark WNT and β -catenin pathway (**b**). Analysis was performed on all tumours of Extended Data Fig. 5a. **c,** The log-transformed fold change in expression of genes involved in WNT signalling ($P < 0.05$) in *Trp53^{-/-}* ($n = 77$) and *Trp53^{+/+}* ($n = 68$) GEMM tumours depicted in Extended Data Fig. 5a. Black bars indicate genes that positively regulate or are generally increased with active WNT signalling. Red bars indicate genes that negatively regulate or are downregulated with active WNT signalling. **d,** Gene set

enrichment analysis (GSEA) for Hallmark pathways in TCGA wild-type *TP53* breast tumours ($n = 643$) versus mutant *TP53* ($n = 351$) human tumours (any *TP53* mutation) or *TP53* loss (based on the IARC TP53 database; see Methods). Normalized enrichment score is shown with the FDR indicated. **e,** Correlation coefficient (R) of all genes involved in WNT signalling that correlate significantly ($P < 0.05$) with mutant *TP53* ($n = 351$) versus wild-type *TP53* ($n = 643$) in TCGA breast tumours. Black bars indicate genes that positively regulate or are generally increased with active WNT signalling. Red bars indicate genes that negatively regulate or are downregulated with active WNT signalling. P values were determined by two-tailed ANOVA with FDR multiple-testing correction (**c, e**).



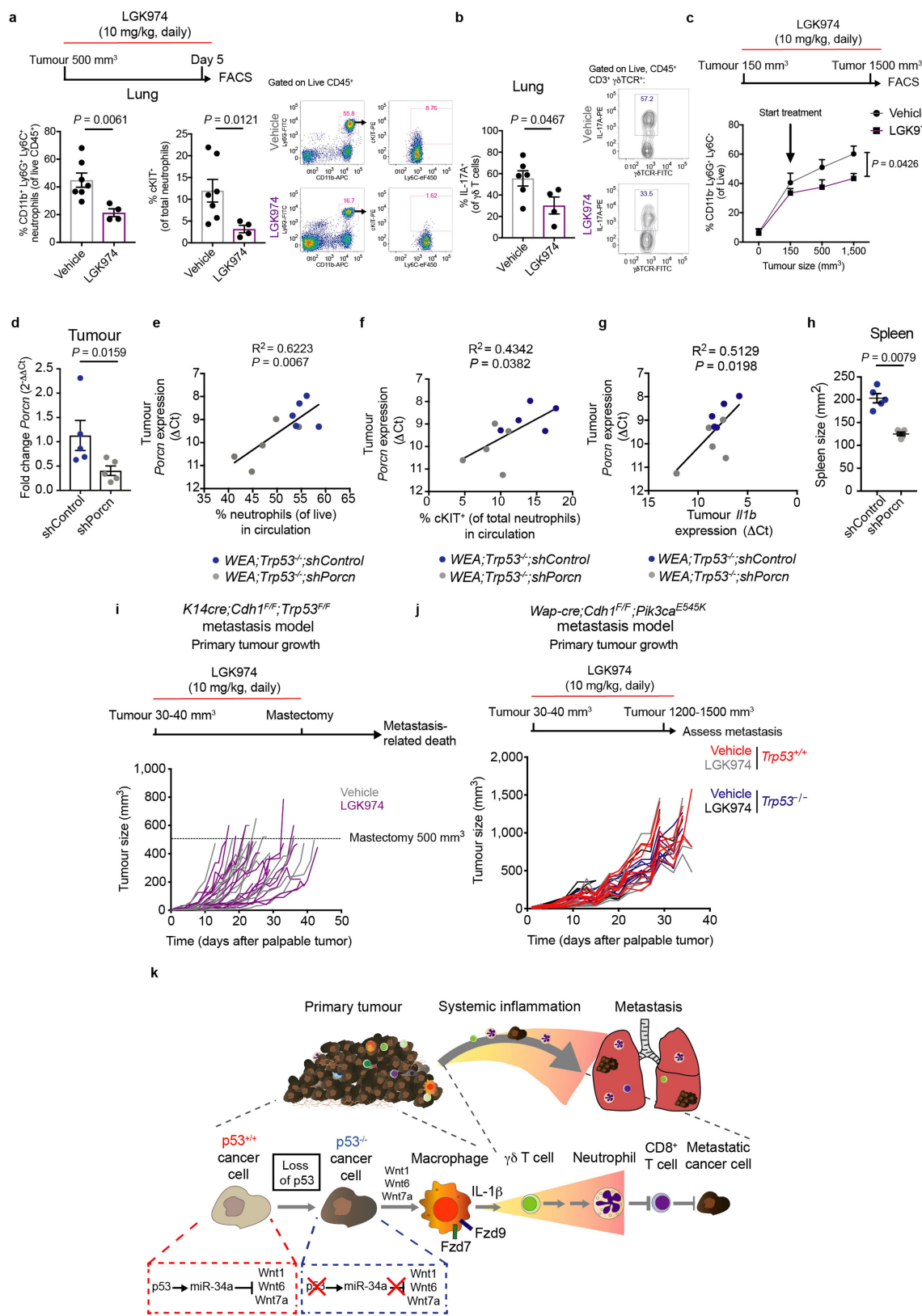
Extended Data Fig. 7 | p53 does not bind the regulatory regions of WNT ligands directly. **a**, ChIP-seq profile of p53 binding to DNA demonstrating enrichment on the *Cdkn1a* (p21) locus in *Trp53*^{+/+} WEA and WEP cell lines (three cell lines from three independent tumours per GEMM). **b**, Absence of p53 binding to *Wnt1*, *Wnt6* or *Wnt7a* loci. **c**, Enrichment of p53 on the miR-34a (*miR-34a*) locus. **d**, RT-qPCR

analysis of *Wnt* ligand expression in *WEA;Trp53*^{+/+} and *WEA;Trp53*^{-/-} cell lines after overexpression (OE) of miR-34a in *WEA;Trp53*^{-/-} cells ($n = 3$ technical replicates per group). Plots are representative of three separate experiments with three technical replicates. All data are mean \pm s.e.m. P values were determined by two-tailed one-way ANOVA with Tukey multiple-testing correction (**d**).



Extended Data Fig. 8 | Macrophages are activated by $T\text{rp}53^{-/-}$ cancer cells via FZD7 and FZD9 receptors in vitro. **a**, The \log_2 -transformed fold change in expression of WNT receptors *Fzd7* and *Fzd9* in bulk tumours comparing $T\text{rp}53^{-/-}$ ($n = 77$) and $T\text{rp}53^{+/+}$ ($n = 68$) GEMM tumours using RNA-seq analysis. **b**, Expression of *FZD7* and *FZD9* in *TP53* wild-type ($n = 643$) and *TP53* mutant ($n = 351$) human breast tumours of the TCGA dataset. **c**, Silencing of *Fzd7* and *Fzd9* in BMDMs after transfection with siRNA pools against both receptors, as determined by RT-qPCR ($n = 6$ biological replicates per group). **d**, Expression of *Il1b* in

BMDMs after exposure to conditioned medium of $T\text{rp}53^{+/+}$ and $T\text{rp}53^{-/-}$ *Wap-cre;Cdh1^{F/F};Akt1^{E17K}* cell lines ($n = 6$ biological replicates per group), as determined by RT-qPCR. Where indicated, BMDMs were transfected with control siRNA or *Fzd7* and *Fzd9* siRNA pools. Data in **a**, **c**, **d** are mean \pm s.e.m. Box plots are as described in Fig. 3e. *P* values were determined by two-tailed one-way ANOVA with FDR multiple-testing correction (**a**), two-tailed Mann–Whitney U-test (**b**) or two-tailed one-way ANOVA with Tukey multiple-testing correction (**d**).



Extended Data Fig. 9 | See next page for caption.

Extended Data Fig. 9 | Pharmacological and genetic targeting of PORCN in p53-deficient tumours reduces systemic inflammation. **a**, Total and cKIT⁺ neutrophil frequencies in lungs of vehicle-treated ($n = 7$) or LGK974-treated ($n = 4$) *K14-cre;Cdh1^{F/F};Trp53^{F/F}* (KEP) mice using indicated 5-day short-term treatment schedule. Representative flow cytometry plots are shown. **b**, Frequency of IL-17A-producing $\gamma\delta$ T cells in lungs of vehicle-treated ($n = 6$) or LGK974-treated ($n = 4$) KEP mice. Representative flow cytometry plots are shown. **c**, Kinetics of circulating neutrophils in vehicle- or LGK974-treated KEP mice using indicated long-term treatment schedule, shown as frequency at indicated tumour volumes ($n = 8$ per group). **d**, RT-qPCR analysis of *Porcn* expression in end-stage bulk tumour ($n = 5$ per group). Data are normalized to control shRNA (shControl) and represents an average of two technical replicates. **e**, Correlation of total neutrophil levels in the circulation with the expression of *Porcn* in *WEA;Trp53^{-/-};shControl* and *WEA;Trp53^{-/-};shPorcn* whole tumour lysate ($n = 5$ per group). **f**, Correlation of cKIT⁺ neutrophil levels in circulation with expression of *Porcn* in *WEA;Trp53^{-/-};shControl* and *WEA;Trp53^{-/-};shPorcn* whole

tumour lysate ($n = 5$ per group). **g**, Correlation of *Porcn* expression and *Il1b* expression in bulk *WEA;Trp53^{-/-};shControl* (blue) and *WEA;Trp53^{-/-};shPorcn* tumours (grey) ($n = 5$ per group). Data represent an average of two technical replicates. **h**, Spleen area in mice with *WEA;Trp53^{-/-};shControl* (blue) and *WEA;Trp53^{-/-};shPorcn* tumours (grey) tumours at end stage ($n = 5$ per group). **i**, Growth kinetics of orthotopically transplanted KEP mammary tumours, treated with vehicle ($n = 12$) or LGK974 ($n = 15$). Each line represents an individual mouse. **j**, Growth kinetics of orthotopically injected *Trp53^{+/+}* and *Trp53^{-/-}* WEP cells, treated with vehicle or LGK974. Each line represents an individual mouse ($n = 9$ per group). **k**, Schematic representation of the findings of this study: loss of p53 in breast cancer cells triggers secretion of WNT ligands to activate tumour-associated macrophages. This stimulates systemic expansion and activation of neutrophils, which we have previously shown to be immunosuppressive⁵, thus driving metastasis. All data are mean \pm s.e.m. *P* values are determined by two-tailed Mann–Whitney *U*-test (**a–d, h**), linear regression analysis (**e–g**) and area under the curve of average growth curves, followed by two-tailed Welch's *t*-test (**i, j**).

Reporting Summary

Nature Research wishes to improve the reproducibility of the work that we publish. This form provides structure for consistency and transparency in reporting. For further information on Nature Research policies, see [Authors & Referees](#) and the [Editorial Policy Checklist](#).

Statistical parameters

When statistical analyses are reported, confirm that the following items are present in the relevant location (e.g. figure legend, table legend, main text, or Methods section).

n/a Confirmed

- The exact sample size (n) for each experimental group/condition, given as a discrete number and unit of measurement
- An indication of whether measurements were taken from distinct samples or whether the same sample was measured repeatedly
- The statistical test(s) used AND whether they are one- or two-sided
Only common tests should be described solely by name; describe more complex techniques in the Methods section.
- A description of all covariates tested
- A description of any assumptions or corrections, such as tests of normality and adjustment for multiple comparisons
- A full description of the statistics including central tendency (e.g. means) or other basic estimates (e.g. regression coefficient) AND variation (e.g. standard deviation) or associated estimates of uncertainty (e.g. confidence intervals)
- For null hypothesis testing, the test statistic (e.g. F , t , r) with confidence intervals, effect sizes, degrees of freedom and P value noted
Give P values as exact values whenever suitable.
- For Bayesian analysis, information on the choice of priors and Markov chain Monte Carlo settings
- For hierarchical and complex designs, identification of the appropriate level for tests and full reporting of outcomes
- Estimates of effect sizes (e.g. Cohen's d , Pearson's r), indicating how they were calculated
- Clearly defined error bars
State explicitly what error bars represent (e.g. SD, SE, CI)

Our web collection on [statistics for biologists](#) may be useful.

Software and code

Policy information about [availability of computer code](#)

Data collection

Flow cytometry data: data acquisition was performed on BD LSRII flow cytometer using Diva software (BD Biosciences) or Beckman Coulter CyAn ADP flow cytometer with Summit software.
 For RNAseq of murine tumours: sequenced using the Illumina Hiseq2000/Hiseq2500 Machine
 For IHC: for individual images, cellSens Entry software (Olympus). For digital processing, slides were scanned using the Aperio ScanScope (Aperio, Vista, CA).
 Cell growth kinetics in vitro were analysed using the IncuCyte System (Essen BioScience).
 For RT-qPCR: LightCycler 480 thermocycler (Roche).
 For western blot: Odyssey CLx imaging system

Data analysis

Statistical analyses were performed using GraphPad Prism 7/8 (GraphPad Software Inc., La Jolla, CA). Flow cytometry data analysis was performed using FlowJo software version 9.9. For images: ImageJ software 1.48v. For the mouse RNA-Seq/human TCGA analysis: R software version 3.4.2, Tophat2 (Tophat version 2.1.0 / Bowtie version 1.0.0), edgeR R package version 3.20.5, biomaRt R package, NMF R-package version 0.20.6, Ingenuity Pathway analysis version 01-06 (QIAGEN), flexgsea R package and R2 Genomics Analysis and Visualization Platform (<http://r2.amc.nl/>) were used. Principal component analysis was performed using the pcomp-function in R (version 3.4.2). For ChIP-sequencing: Easeq software was used for visualisation. For power calculations and group size determination: G*Power software (version 3.1).

For manuscripts utilizing custom algorithms or software that are central to the research but not yet described in published literature, software must be made available to editors/reviewers upon request. We strongly encourage code deposition in a community repository (e.g. GitHub). See the Nature Research [guidelines for submitting code & software](#) for further information.

Data

Policy information about [availability of data](#)

All manuscripts must include a [data availability statement](#). This statement should provide the following information, where applicable:

- Accession codes, unique identifiers, or web links for publicly available datasets
- A list of figures that have associated raw data
- A description of any restrictions on data availability

The RNA sequencing datasets have been deposited in the Gene Expression Omnibus (GEO, NCBI) repository under accession number GSE112665.

Field-specific reporting

Please select the best fit for your research. If you are not sure, read the appropriate sections before making your selection.

Life sciences Behavioural & social sciences Ecological, evolutionary & environmental sciences

For a reference copy of the document with all sections, see nature.com/authors/policies/ReportingSummary-flat.pdf

Life sciences study design

All studies must disclose on these points even when the disclosure is negative.

Sample size

Sample size was based on previous experience with the mouse models (Coffelt et al., 2015; Doornetal et al., 2013) or otherwise determined using G*Power software version 3.1. For immunohistochemistry, flow cytometry and RT-qPCR experiments, ≥3 biological replicates were used. For the intervention experiment assessing metastasis, ≥ 9 mice were used. To exclude bias towards one particular GEMM in the analyses for Figure 1, we have performed the same analyses on the average of the neutrophil levels and serum cytokine values per model. This demonstrated the same correlations between the assessed values and p53 status of the tumour, thus excluding bias towards one or several particular models.

Data exclusions

Mice with skin tumours (in the models in which Keratin-14 (K14) drives expression of Cre recombinase, skin tumours can arise, since K14 is also expressed in the skin) were excluded from the study, based on assessment of H&E stainings of the tumour. For orthotopic transplantation of cancer cell lines, samples were excluded when not properly transplanted in the mammary fat pad (e.g. in the skin adjacent to the mammary gland). For metastasis scoring in the KEP-tumour based metastasis model, mice that died because of reasons not related to metastasis were excluded (surgery-related or local recurrence of the primary tumour after surgery). In the WEP cell line-based metastasis model, samples were excluded when smaller tumours, due to their invasive behaviour, grew through the skin before the end of the experiment (1200 - 1500 mm³ tumour size), to allow all tumours sufficient time to metastasize. For RT-PCR analysis, samples were run in technical duplicate and if the difference between the Ct values of the duplo was bigger than 1 cycle, samples were discarded. Exclusion criteria were pre-determined before the experiments.

Replication

In vitro experiments were repeated in at least 2 - 3 independent experiments and showed comparable results between experiments.

Randomization

For intervention studies, mice were randomly distributed over the two treatment arms when tumours reached the size indicated in the figures. The first animal was assigned randomly in the treatment or control group, after which each subsequent animal was placed in the next group.

Blinding

Tumour measurements and post mortem analyses were performed in a blinded fashion. Assessment of IHC counts were performed by 2 or more independent researchers in a blinded fashion.

Reporting for specific materials, systems and methods

Materials & experimental systems

n/a	Involved in the study
<input type="checkbox"/>	<input checked="" type="checkbox"/> Unique biological materials
<input type="checkbox"/>	<input checked="" type="checkbox"/> Antibodies
<input type="checkbox"/>	<input checked="" type="checkbox"/> Eukaryotic cell lines
<input checked="" type="checkbox"/>	<input type="checkbox"/> Palaeontology
<input type="checkbox"/>	<input checked="" type="checkbox"/> Animals and other organisms
<input checked="" type="checkbox"/>	<input type="checkbox"/> Human research participants

Methods

n/a	Involved in the study
<input type="checkbox"/>	<input checked="" type="checkbox"/> ChIP-seq
<input type="checkbox"/>	<input checked="" type="checkbox"/> Flow cytometry
<input checked="" type="checkbox"/>	<input type="checkbox"/> MRI-based neuroimaging

Unique biological materials

Policy information about [availability of materials](#)

Obtaining unique materials

Biological samples derived from the mouse model are available upon reasonable request and after signing of a standard MTA.

Antibodies

Antibodies used

For a list of used antibodies, also see Supplemental Table 1.

- Flow cytometry:

CD45 eFluor 605NC eBioscience/ThermoFisher 93-0451 1:100
 CD45 BUV395 30-F11 BD Biosciences 564279 1:200
 CD11b BV650 M1/70 BioLegend 101239 1:400
 CD11b APC M1/70 eBioscience/ThermoFisher 17-0112-81 1:400
 CD11b APC-eFluor 780 M1/70 eBioscience/ThermoFisher 47-0112-82 1:400
 Ly6G APC 1A8 eBioscience/ThermoFisher 17-9668-82 1:400
 Ly6G FITC 1A8 BD Biosciences 561105 1:400
 Ly6C eFluor 450 HK1.4 eBioscience/ThermoFisher 48-5932-82 1:400
 F4/80 APC-eFluor 780 BM8 eBioscience/ThermoFisher 47-4801-82 1:400
 F4/80 APC BM8 eBioscience/ThermoFisher 17-4801-82 1:400
 F4/80 FITC BM8 eBioscience/ThermoFisher 11-4801-82 1:400
 cKIT PE 2B8 eBioscience/ThermoFisher 12-1171-82 1:200
 cKIT PE-Cy7 2B8 eBioscience/ThermoFisher 25-1171-82 1:200
 CD3 PE-Cy7 145-2C11 eBioscience/ThermoFisher 25-0031-82 1:200
 CD4 APC-eFluor 780 GK1.5 eBioscience/ThermoFisher 47-0041-82 1:200
 CD8 APC-eFluor 780 53-6.7 eBioscience/ThermoFisher 47-0081-82 1:400
 CD8 PerCP-eFluor 710 53-6.7 eBioscience/ThermoFisher 46-0081-82 1:400
 Gamma delta-TCR FITC GL3 BD Biosciences 553177 1:400
 CD19 APC-eFluor 780 eBio1D3 eBioscience/ThermoFisher 47-0193-82 1:200
 CD34 eFluor 450 RAM34 eBioscience/ThermoFisher 48-0341-82 1:100
 CD16/32 PerCP-eFluor 710 93 eBioscience/ThermoFisher 46-0161-82 1:200
 Sca-1 PE D7 eBioscience/ThermoFisher 12-5981-82 1:100
 CD45R APC-eFluor 780 RA3-6B2 eBioscience/ThermoFisher 47-0452-82 1:200
 CD5 APC-eFluor 780 53-7.3 eBioscience/ThermoFisher 47-0051-82 1:200
 CD127 APC-eFluor 780 A7R34 eBioscience/ThermoFisher 47-1271-82 1:200
 Ter119 APC-eFluor 780 TER-119 eBioscience/ThermoFisher 47-5921-82 1:200
 CCR2 AF700 475301 R&D Systems FAB5538N 1:200
 CCR6 BV421 29-2L17 BioLegend 129817 1:200
 CD206 AF488 MR5D3 AbD Serotec/Bio-Rad MCA2235 1:200
 CSF-1R PE AFS98 eBioscience/ThermoFisher 12-1152-82 1:200
 CXCR4 PerCP-eFluor 710 2B11 eBioscience/ThermoFisher 46-9991-82 1:200
 MHC-II APC-eFluor 780 M5/114.15.2 eBioscience/ThermoFisher 47-5321-82 1:200
 CD68 BV421 Y1/82A BD Biosciences 564943 1:200
 CD14 BUV737 M5E2 BD Biosciences 564444 1:400
 CD206 FITC 15-2 BioLegend 321103 1:200
 CD168 APC GHI/61 BioLegend 333609 1:200
 HLA-DR BV650 G46-6 BD Biosciences 564231 1:200
 - Western blotting:
 :p53 1C12 Cell Signalling 2524 1:1000
 p21 SX118 BD Biosciences 556430 1:1000
 Wnt1 10C8 EMD Millipore MABD168 1:1000
 Wnt6 Polyclonal (EPR9244) Abcam Ab154144 1:1000
 Wnt7a Polyclonal Novus Biologicals NBP2-20913 1:1000
 Porcupine Polyclonal Novus Biologicals NBP1-79322 1:1000
 Non-phospho- β -catenin - 8E7 EMD Millipore 05-665 1:1000
 β -actin D6A8 Cell Signalling 8457 1:5000

β -actin A1978 Sigma A2228 1:5000
 GAPDH - 6C5 HyTest 5G4 1:5000
 Donkey-anti-mouse IgG IRDye 680RD LiCor 926-68072 1:10000
 Donkey-anti-rabbit IgG IRDye 800CW LiCor 926-32213 1:10000
 - Immunohistochemistry:
 Ly6G 1A8 BD Biosciences 551459 1:150
 F4/80 CI:A3-1 AbD Serotec/Bio-Rad MCA497GA 1:400
 CD8 4SM15 eBioscience/ThermoFisher 14-0808-82 1:2000
 CD4 4SM95 eBioscience/ThermoFisher 14-9766-82 1:1000
 Foxp3 FJK-16s eBioscience/ThermoFisher 14-5773-82 1:400
 Cytokeratin-8 Troma-I DSHB University of Iowa TROMA-I 1:600
 Goat-anti-Rat IgG - 3052-08 SouthernBiotech 3052-08 1:100
 - Chromatin immunoprecipitation:
 p53 5 μ g 1C12 Cell Signalling 2524

Validation

Antibodies for flow cytometry were validated for target species (mouse or human) using FMO or isotype controls where necessary.
 Antibodies used for IHC were validated for mouse by the Pathology facilities at the NKI.

Eukaryotic cell lines

Policy information about [cell lines](#)

Cell line source(s)

Mouse cell lines were generated in house.
 MCF-7 and HEK293T cells were provided by the Schumacher lab (Netherlands Cancer Institute).

Authentication

Mouse tumour-derived cell lines were checked for purity using genotyping.
 MCF-7 cells were not authenticated, but the TP53-WT and TP53-KO cells were made from the same parental line.

Mycoplasma contamination

Cells were routinely tested for mycoplasma contamination and only negative cells were used.

Commonly misidentified lines
(See [ICLAC](#) register)

No commonly misidentified lines were used in this study.

Animals and other organisms

Policy information about [studies involving animals; ARRIVE guidelines](#) recommended for reporting animal research

Laboratory animals

The following mouse models were used in this study: Keratin14 (K14)-cre;Cdh1F/F;Trp53F/F, K14cre;Trp53F/F, K14cre;Brca1F/F;Trp53F/F, Whey Acidic Protein (Wap)-cre;Trp53F/F, Wap-cre;Brca1F/F;Trp53F/F, Wap-cre;Brca1F/F;Trp53F/F;Col1a1invCAG-Met-IRES-Luc/+ (Wap-cre;Brca1F/F;Trp53F/F;Met), Wap-cre;Brca1F/F;Trp53F/F;Col1a1invCAG-Myc-IRES-Luc/+ (Wap-cre;Brca1F/F;Trp53F/F;Myc), Wap-cre;Brca1F/F;Trp53F/F;Col1a1invCAG-Myb2-IRES-Luc/+ (Wap-cre;Brca1F/F;Trp53F/F;Myb2), Wap-cre;Trp53F/F;Col1a1invCAG-ESR1-IRES-Luc/+ (Wap-cre;Trp53F/F;HA-ESR1), Wap-cre;Cdh1F/F;Col1a1invCAG-AktE17K-IRES-Luc/+ (Wap-cre;Cdh1F/F;AktE17K), Wap-cre;Cdh1F/F;Col1a1invCAG-Pik3caE545K-IRES-Luc/+ (Wap-cre;Cdh1F/F;Pik3caE545K), Wap-cre;Cdh1F/F;Col1a1invCAG-Fgfr2ex1-15-IRES-Luc/+ (Wap-cre;Cdh1F/F;Fgfr2ex1-15), Wap-cre;Cdh1F/F;T2/Onc;Rosa26Lox66SBLox71/+ (Wap-cre;Cdh1F/F;SB), Wap-cre;Map3k1F/F;PtenF/F, Mouse mammary tumour virus LTR (MMTV)-NeuT40. All mouse models were on FVB/N background, except MMTV-NeuT and Wap-cre;Cdh1F/F;SB, which were on Balb/c and a mixed genetic (C57BL/6J and FVB/N) background, respectively. Mice developed tumours between 3 and 18 months of age. For tumour inoculation experiments, FVB/N mice were used of 8 - 10 weeks of age. All used mice were female. All materials were derived from one or more of the above models.

Wild animals

This study did not involve wild animals.

Field-collected samples

This study did not involve field-collected samples.

ChIP-seq

Data deposition

Confirm that both raw and final processed data have been deposited in a public database such as [GEO](#).

Confirm that you have deposited or provided access to graph files (e.g. BED files) for the called peaks.

Data access links

May remain private before publication.

The data of the ChIP-seq experiments were used to assess specific loci, and not to make statements on genome-wide chromatin binding of p53. For this reason we did not upload the files to GEO. The data is available upon request.

Files in database submission

See above.

Genome browser session
(e.g. [UCSC](#))

https://genome.ucsc.edu/cgi-bin/hgTracks?hgS_doOtherUser=submit&hgS_otherUserName=sprekovic&hgS_otherUserSessionName=p53%20mm10

Methodology

Replicates	Two cell lines, derived from spontaneous mouse tumours, Wap-cre;Cdh1F/F;Akt-E17K and Wap-cre;Cdh1F/F;Pik3ca-E545K, were used. Of each of these lines, three cell lines from three individual mouse tumours were used as biological replicates.
Sequencing depth	Number of reads per sample were approximately between 1.0×10^7 - 2.0×10^7 . Details of sequencing metric (total number of reads and number of unmapped reads) per sample are available upon request. Single-end, 65-bp reads were used.
Antibodies	p53 antibody (clone 1C12, #2524, Lot 13, Cell Signalling) was used for ChIP experiments.
Peak calling parameters	Peak calling over input control was performed using MACS 2.0 peak caller (callpeak -t P1.bam -c InputP1.bam -f BAM -g mm -n P1tumor -B -q 0.01).
Data quality	Quality control measurements including count in peaks for all the samples, plots indicating all the called peaks and their respective fold enrichments and q-values, Venn diagrams showing the overlap of peaks are available upon request.
Software	Data was visualized using Easeq software.

Flow Cytometry

Plots

Confirm that:

- The axis labels state the marker and fluorochrome used (e.g. CD4-FITC).
- The axis scales are clearly visible. Include numbers along axes only for bottom left plot of group (a 'group' is an analysis of identical markers).
- All plots are contour plots with outliers or pseudocolor plots.
- A numerical value for number of cells or percentage (with statistics) is provided.

Methodology

Sample preparation	Flow cytometry analysis was performed as previously described ⁶ . Briefly, tissues were collected in ice-cold PBS and blood was collected in tubes containing heparin. Tumours and lungs were mechanically chopped using a McIlwain tissue chopper (Mickle Laboratory Engineering). Tumours were digested for 1 hour (h) at 37°C in 3 mg/mL collagenase type A (Roche) and 25 µg/mL DNase (Sigma) in serum-free DMEM medium. Lungs were digested for 30 minutes (min) at 37°C in 100 µg/mL Liberase TM (Roche). Enzyme reactions were stopped by addition of cold DMEM/8% Fetal Calf Serum (FCS) and suspensions were dispersed through a 70 µm cell strainer. Bone marrow was collected from the tibia and femurs of both hind legs and flushed using RPMI/8% FCS through a 70 µm cell strainer. Single-cell suspensions were treated with NH4Cl erythrocyte lysis buffer. Before staining, cell suspensions were subjected to Fc receptor blocking (rat anti-mouse CD16/32, BD Biosciences) for 15 min at 4°C, except for bone marrow (to allow assessment of CD16/32 expression). Cells were stained with conjugated antibodies for 30 min at 4°C in the dark in PBS/0.5% BSA. 7AAD (1:20; eBioscience) or Fixable Viability Dye eFluor 780 (1:1000; eBioscience) was added to exclude dead cells. For intracellular cytokine staining, single-cell suspensions were stimulated in IMDM containing 8% FCS, 100 IU/mL penicillin, 100 mg/mL streptomycin, 0.5% β-mercaptoethanol, 50 ng/ml PMA, 1 mM ionomycin and Golgi-Plug (1:1,000; BD Biosciences) for 3h at 37°C. Surface antigens were stained first, followed by fixation and permeabilization using the Cytofix/Cytoperm kit (BD Biosciences) and staining of intracellular proteins.
Instrument	All experiments were performed using a BD LSR II flow cytometer using Diva software or the Beckman Coulter CyAn ADP flow cytometer using Summit software.
Software	The software used to collect data was Diva software (BD Biosciences) and data analysis was performed using FlowJo software version 9.9.
Cell population abundance	No sorting of cells was performed.
Gating strategy	The morphologic gate (FSC/SSC) was used to included all cells and excluding debris. Doublets (using FSC-H/FSC-A and SSC-H/SSC-A) and dead cells were excluded. Immune cells were then gated based on their specific markers, indicated in relevant figures. Gating strategies are shown in Extended Data Fig. 2 and 3.

- Tick this box to confirm that a figure exemplifying the gating strategy is provided in the Supplementary Information.